AGU PUBLICATIONS

Tectonics

RESEARCH ARTICLE
10.1002/2013TC003372

Key Points:
- We have made accurate measurements of residual depth of old oceanic floor
- Our measurements have key implications for dynamic topography
- There are major discrepancies between our results and model predictions

Correspondence to:
N. White,
njw10@cam.ac.uk

Citation:
Winterbourne, J., N. White, and A. Crosby (2014), Accurate measurements of residual topography from the oceanic realm, *Tectonics*, *33*, 982–1015, doi:10.1002/2013TC003372.

Received 20 MAY 2013
Accepted 25 APR 2014
Accepted article online 13 MAY 2014
Published online 10 JUN 2014

Accurate measurements of residual topography from the oceanic realm

Jeffrey Winterbourne[1], Nicky White[2], and Alistair Crosby[1]

[1]BP Exploration Operating Company Limited, Sunbury-on-Thames, UK [2]Bullard Laboratories, Department of Earth Sciences, University of Cambridge, Cambridge, UK

Abstract In the oceans, our understanding of plate subsidence as a function of age permits residual depth anomalies to be identified and mapped. These anomalies may reflect dynamic topography and could be an important means for constraining convective circulation of the sublithospheric mantle. Here we analyze a global database of seismic reflection and wide-angle profiles from heavily sedimented oceanic crust, which abuts continental lithosphere. At 449 locations, we calculated water-loaded subsidence, compared it with a reference age-depth relationship, and determined residual depth. We then combined these spot measurements of residual depth with observations from mid-oceanic ridges and from selected ship track bathymetry to construct a global map of residual depth. Our results suggest that the amplitude of residual depth varies by up to ±1 km with wavelengths of order 10^3 km. We compare our residual depths with free-air gravity and seismic tomographic anomalies. Our results show that residual depths correlate with long-wavelength gravity anomalies. In contrast, correlations between residual depths and vertically averaged shear velocity anomalies within the upper and/or the lower mantle are weaker. The largest discrepancies occur at short (~1000 km) wavelengths. These combined observations suggest that residual depth anomalies could be generated by density variations within a thin (~10^2 km) low-viscosity layer beneath the lithosphere. Our global compilation should play a significant role in helping to refine predictive geodynamical models.

1. Introduction

Changing patterns of convective circulation within the Earth's mantle generate and maintain dynamic topography, which is some fraction of observed topography (Figure 1) [*Hager et al.*, 1985; *Hager and Richards*, 1989; *Cazenave et al.*, 1989]. Since convective circulation cannot be directly observed, detailed measurements of dynamic topography through space and time should provide useful physical constraints. The principal problem is that it is difficult to discriminate between small dynamic topographic signals, which are probably driven by density changes beneath the lithospheric plate, and larger isostatic signals, which are generated by density changes within the crust and lithosphere caused by thermal and compositional heterogeneity. This problem of discrimination is especially acute within the continents where density structure is both poorly known and spatially variable. Fortunately, spatial patterns of dynamic topography are easier to measure within the oceanic realm since isostatic signals can be removed with greater confidence. Oceanic lithosphere cools, thickens, and subsides as a function of age away from the mid-oceanic ridge [*Parsons and Sclater*, 1977]. The relationship between plate subsidence and age in regions, which have negligible dynamic topography, is well known [e.g., *Crosby et al.*, 2006]. Consequently, it is possible to use regional age-depth observations to determine positive and negative residual depth anomalies. These anomalies have several possible explanations. A strict definition of dynamic topography states that it is the deflection of the Earth's surface in response to normal stresses, which are generated by flow within the convecting mantle [e.g., *Flament et al.*, 2013]. Since residual depth anomalies can be generated by thermal anomalies located either within the thermal boundary layer or within the convecting mantle, the size and shape of these anomalies yield an upper limit for dynamic topography in a strict sense. A broader and more practical definition of dynamic topography embraces thermochemical and flow-related anomalies beneath the lithospheric plate.

In recent years, different maps, which show the global variation of residual topography in the oceanic realm, have been published [e.g., *Colin and Fleitout*, 1990; *Panasyuk and Hager*, 2000; *Kaban et al.*, 2003; *Crosby et al.*, 2006; *Crosby and McKenzie*, 2009; *Flament et al.*, 2013]. We wish to revisit this topic for two important

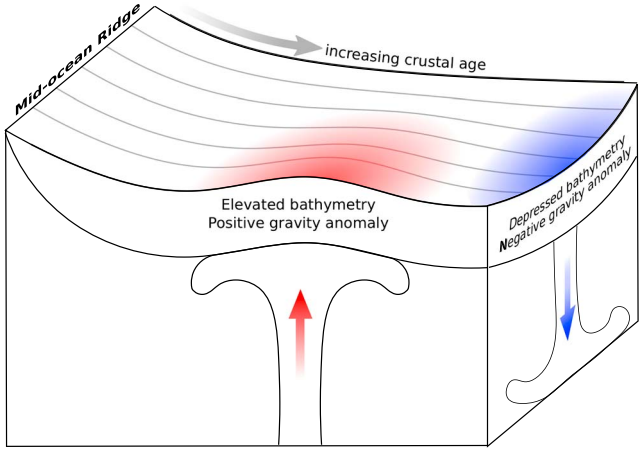

Figure 1. Cartoon summarizing main controls of depth to oceanic basement as function of plate age. General increase in plate thickness with age is controlled by cooling and thickening of lithospheric mantle [e.g., *Crosby et al.*, 2006]. Negative and positive depth anomalies are caused by convective upwellings and downwellings, respectively. Red patch underlain by upward pointing red arrow = convective upwelling and its surficial manifestation; blue patch underlain by downward pointing blue arrow = convective downwelling and its surficial manifestation.

reasons. First, a large body of modern seismic reflection and wide-angle profiles have been acquired over the last 10 years along the margins of, and within, oceanic basins. These profiles can be used to accurately calculate water-loaded subsidence in places with thick sedimentary cover and variable crustal thickness. Age-depth analyses have mostly been carried out on ship track bathymetry from regions such as the Pacific plate, which have little or no sedimentary cover. We can enlarge this database by including age-depth measurements from older (> 60 Ma) oceanic crust adjacent to continental margins where sedimentary thicknesses are significantly larger. These additional measurements help to constrain the spatial variation of dynamic topography on adjacent continents. Second, the age-depth relationship has been reanalyzed by *Crosby et al.* [2006] using a global database of ship track bathymetry. In contrast to earlier studies, and as far as is practicable, these authors excised oceanic plateaux and regions of positive and negative residual topography, using long-wavelength gravity anomalies as a proxy for dynamic support. Consequently, their age-depth relationship is a more robust starting point for estimating residual depth anomalies, provided crustal thickness is known. Previous age-depth syntheses tend to be biased toward regions with negative dynamic topography and/or with anomalously thickened crust (Figure 4a). For example, *Parsons and Sclater* [1977] deliberately maximized depth estimates for ages greater than 60 Ma in order to demonstrate that oceanic plates do not subside by half-space cooling. In contrast, *Stein and Stein* [1992] did not excise regions with thickened oceanic crust, which biases their age-depth estimates toward shallow values. For these reasons, neither of these popular age-depth compilations have been used to estimate residual depths.

We have built a large database of seismic reflection and wide-angle profiles acquired by the hydrocarbon industry and by the academic community (Appendix A). This database is concentrated along edges of passive continental margins in the Atlantic, Indian, and Southern Oceans. For completeness, we include profiles from convergent margins, which fringe the Pacific Ocean and elsewhere. Our principal concern is to show that this database can be used in a transparent way to obtain accurate measurements of residual depth. Our measurements have been augmented by reanalyzing residual depth along the mid-oceanic ridge system and throughout the oceans where sedimentary thickness is negligible and where oceanic plateaux are absent.

Our goal is to create a global map of residual depth based upon accurate spot measurements. The simplest and quickest approach is to exploit published gridded databases of bathymetry, sediment thickness, and crustal thickness [e.g., *Smith and Sandwell*, 1997; *Divins*, 2008; *Bassin et al.*, 2000]. For example, *Müller et al.* [2008] and *Crosby and McKenzie* [2009] use these grids to make maps of residual topography for the oceans. Inevitably, these maps are poorly constrained in areas of thick sediment, and there is no discrimination between depth anomalies caused by changes in crustal thickness and those caused by subplate processes. On old oceanic floor, sedimentary and crustal thickness corrections are especially large and need to be carefully measured. Although global bathymetric grids are well constrained *Smith and Sandwell* [1997], digital grids of sedimentary thickness are unreliable. A well-known digital sedimentary thickness grid has been published by the National Geophysical Data Center [*Divins*, 2008]. This grid has significant errors at continental margins, which arise from the requirement to interpolate between sparse measurements. At thickly

sedimented passive margins, there are discrepancies of up to 3.5 km [*Winterbourne et al.*, 2009]. Global grids of crustal thickness also have variable resolution (e.g., CRUST 2.0) [*Bassin et al.*, 2000].

2. Data Sources

Observational constraints are grouped into two categories (Table 1). The larger category consists of two-dimensional deep seismic reflection profiles, which cross continental margins and terminate on oceanic crust. They are mostly of excellent quality but an obvious drawback is that they are recorded in two-way travel time. The smaller category consists of densely sampled and reversed seismic wide-angle profiles. In both cases, two criteria are used to ensure that we are dealing with *bona fide* oceanic floor. First, the three-layer structure of oceanic crust is easily identifiable on modern seismic wide-angle and reflection profiles (e.g., Figure 3). Second, we exploit a global database of crustal age determined from magnetic anomalies [*Müller et al.*, 2008]. Both criteria are conservatively applied at margins where it can be difficult to discriminate between thinned continental crust and oceanic crust. Crucially, seismic reflection and wide-angle profiles intersect at 39 locations on oceanic crust. These intersections can be used to construct an empirical relationship between two-way travel time and thickness for the sedimentary column, which yields reliable isostatic corrections for sedimentary columns as thick as 10 km [*Czarnota et al.*, 2013].

To augment these spot measurements, we exploited four additional sources of data. First, the global mid-oceanic ridge system is an excellent "plumb line" for estimating residual depth, provided care is taken to correct, where possible, for crustal thickness. Second, we collated ship track bathymetric measurements from *Smith and Sandwell* [1997] which were corrected for sediment loading using the National Geophysical Data Center (NGDC) sedimentary thickness grid [*Divins*, 2008]. We only included ship tracks where sediment thickness is less than 1500 m, and we carefully excised regions where thickened crust occurs. Third, we extracted a small number of residual depth measurements from flexed oceanic plates adjacent to subduction zones. These values were corrected for flexural bending using the results of *Levitt and Sandwell*'s [1995] and *Bry and White*'s [2007] inverse modeling. Finally, *Wheeler and White* [2000] used a combination of age-depth observations from multiple fragments of oceanic crust to estimate minimum residual depths across Southeast Asia. We have included their results in our global compilation (Appendix A).

3. Methodology

Seismic reflection profiles are recorded in two-way travel time, t, and where wide-angle velocity control is not available, we must convert two-way travel time to depth. The average acoustic velocity of the water column is 1500 m s^{-1}, but the average velocity of the sedimentary column, $\bar{v}(z)$, depends upon lithology and upon the degree of compaction. The relationship between two-way travel time and velocity is given by

$$t = 2\int_0^z \frac{\mathrm{d}z}{\bar{v}(z)}, \tag{1}$$

where

$$\frac{1}{\bar{v}(z)} = \frac{\phi}{v_w} + \frac{1-\phi}{v_s}. \tag{2}$$

$v_w = 1.5$ km s^{-1} and $v_s = 5.5$ km s^{-1} are the velocities of sea water and quartz grains, respectively. If we assume that

$$\phi = \phi_\circ \exp(-z/\lambda), \tag{3}$$

where $\phi_\circ$ is the initial porosity and λ is the compaction decay length, we obtain

$$t/2 = \frac{z}{v_s} + \phi_\circ \lambda \left[\frac{1}{v_w} - \frac{1}{v_s}\right] \{1 - \exp(-z/\lambda)\}. \tag{4}$$

Values of $\phi_\circ$ and λ depend upon lithology. Without borehole data, an empirical approach exploits a compilation of 39 coincident seismic reflection and wide-angle profiles, where t and z are known (Figure 2a) [*Winterbourne et al.*, 2009; *Czarnota et al.*, 2013]. This compilation was parameterized using equation (4) for $\phi_\circ = 0.56$ and $\lambda = 4.5$ km. The average density of a sedimentary column on oceanic crust is

$$\bar{\rho} = \rho_s + \frac{\phi_\circ \lambda}{z}(\rho_w - \rho_s)\{1 - \exp(-z/\lambda)\}, \tag{5}$$

Table 1. Profiles Recorded in Two-Way Travel Time

Profile	Reference	Longitude	Latitude	T_w, ms	T_s, ms	T_c, ms	Age, Ma	Z_{wl}, m	Z_{res}, m
1	*Stagg et al.* [2004a]	114.81	−15.61	7378	846	2228	154	6242	−545
2	*Carbotte et al.* [2008]	231.93	47.78	3615	390	2024	3	2948	201
3	*Carbotte et al.* [2008]	229.59	48.29	3852	144	2125	4	3001	271
4	*Stagg et al.* [2004a]	108.53	−20.73	6632	416	2683	127	5637	−88
5	Proprietary data	110.74	−22.04	6734	1192	2260	129	6042	−467
5	Proprietary data	110.40	−22.53	6737	1427	2012	129	6070	−493
6	*Ball* [2005]	137.59	−38.87	6624	265	no data	41	5169	−395
7	*Stagg et al.* [2004a]	109.81	−17.40	7350	270	2764	127	6114	−561
7	*Stagg et al.* [2004a]	110.23	−17.68	7044	282	2841	146	5942	−261
8	*Stagg et al.* [2004a]	109.61	−18.00	7135	174	2843	127	5930	−384
9	*Stagg et al.* [2004a]	108.97	−18.54	7394	129	2809	127	6068	−523
10	*Stagg et al.* [2004a]	108.63	−19.02	7252	389	2398	125	5905	−384
11	*Stagg et al.* [2004a]	111.08	−17.21	6966	121	3194	153	5980	−285
11	*Stagg et al.* [2004a]	110.89	−17.61	6491	260	3554	153	5951	−256
12	*Stagg et al.* [2004a]	110.46	−16.28	7525	390	2406	145	6116	−439
13	*Stagg et al.* [2004a]	110.59	−16.80	7480	267	2523	151	6061	−370
14	*Stagg et al.* [2004a]	114.81	−15.50	7501	658	2283	154	6226	−529
15	*Ball* [2005]	132.24	−37.03	7363	690	no data	68	6045	−673
15	*Ball* [2005]	132.49	−37.52	7350	260	no data	54	5709	−659
16	*Ball* [2005]	129.48	−36.90	6483	613	no data	67	5327	13
17	Proprietary data	5.73	2.55	4034	3603	no data	100	5784	−318
17	Proprietary data	5.72	2.35	4323	3025	no data	99	5554	−82
18	*Ball* [2005]	131.47	−61.88	5970	2015	no data	54	6011	−950
18	*Ball* [2005]	131.50	−62.72	5778	2376	no data	73	6144	−654
19	*Ball* [2005]	139.85	−60.99	5900	967	no data	44	5159	−308
20	Proprietary data	5.12	3.16	3754	4040	no data	98	5913	−418
21	Proprietary data	313.28	3.04	3658	5300	1412	102	6372	−928
22	Proprietary data	6.43	2.22	4100	3249	no data	101	5559	−103
23	*Carbotte et al.* [2008]	231.68	46.49	3730	421	2027	2	3059	66
24	*Coffin et al.* [1986]	44.35	−2.15	5170	3074	no data	149	6226	−539
25	*Coffin et al.* [1986]	44.75	−2.42	5500	2823	1657	147	5989	−306
25	*Coffin et al.* [1986]	44.92	−2.54	5589	2749	1697	146	6025	−345
26	*Coffin et al.* [1986]	43.98	−3.21	5202	3161	1653	148	6023	−339
27	*Carbotte et al.* [2008]	230.69	44.75	3758	210	2113	2	2974	69
28	*Carbotte et al.* [2008]	228.72	45.23	4096	0	2104	5	3063	279
29	Proprietary data	126.98	79.58	4426	1695	no data	18	4609	−533
29	Proprietary data	128.36	79.69	4598	1635	no data	30	4692	−209
30	Proprietary data	128.95	79.41	4394	2071	no data	31	4873	−348
31	Proprietary data	130.52	78.80	3941	2707	no data	45	5021	−166
32	*Coffin et al.* [1986]	43.46	−5.13	5453	3023	1618	142	6083	−415
33	Proprietary data	341.19	13.94	4862	2417	no data	169	5489	225
34	Proprietary data	340.95	15.72	4308	2689	no data	163	5283	424
35	Proprietary data	341.12	18.89	3991	3269	no data	167	5493	219
36	Proprietary data	341.28	23.32	4303	3517	no data	168	5918	−205
37	Proprietary data	341.19	23.45	4244	3603	no data	167	5941	−229
38	Proprietary data	341.79	24.88	3892	2664	no data	166	4952	759
39	Proprietary data	341.65	25.61	4302	2090	no data	162	4818	889
40	Proprietary data	11.70	−11.75	4545	1781	no data	119	4764	691
41	Proprietary data	11.53	−12.89	4462	1979	no data	117	4854	587
44	*Austin and Uchupi* [1982]	11.88	−25.93	5250	2173	no data	122	5593	−105
45	*Austin and Uchupi* [1982]	10.58	−22.97	5215	2209	no data	118	5595	−150
46	*Austin and Uchupi* [1982]	13.20	−29.85	4327	2908	no data	124	5466	48
47	*Austin and Uchupi* [1982]	13.70	−31.10	4335	2790	no data	125	5381	145
48	*Austin and Uchupi* [1982]	13.85	−31.29	4340	2821	no data	125	5408	124
49	*Austin and Uchupi*[1982]	16.00	−33.95	5521	1665	no data	131	5407	185
51	Proprietary data	11.31	−12.56	4390	2348	no data	117	5083	356
52	Proprietary data	11.62	−12.88	4263	2378	1538	117	4648	791
53	Proprietary data	11.44	−12.15	4502	2199	no data	118	5052	389
54	Proprietary data	11.58	−12.32	4300	2381	no data	118	5040	404
55	Proprietary data	9.17	−6.14	4784	3960	1391	116	6163	−738
56	Proprietary data	9.58	−6.19	4662	4134	1381	117	6201	−762
57	Proprietary data	9.47	−6.42	4885	3808	1615	117	6260	−828

Table 1. (continued)

Profile	Reference	Longitude	Latitude	T_w, ms	T_s, ms	T_c, ms	Age, Ma	Z_{wl}, m	Z_{res}, m
58	Proprietary data	10.16	−7.21	5098	3489	no data	119	6493	−1037
58	Proprietary data	10.26	−7.83	5321	2889	no data	119	6197	−740
59	Proprietary data	9.52	−6.69	4942	3758	no data	117	6585	−1153
60	Proprietary data	9.97	−6.91	4914	3725	no data	118	6538	−1088
61	Proprietary data	10.05	−6.82	4881	3661	no data	119	6464	−1011
62	Proprietary data	9.76	−6.76	4890	3784	no data	118	6565	−1124
63	Proprietary data	9.57	−6.73	4952	3740	no data	117	6578	−1145
64	Proprietary data	9.65	−7.28	5226	3309	no data	117	6450	−1016
65	Proprietary data	9.39	−6.77	5037	3687	no data	116	6601	−1174
66	Proprietary data	9.21	−6.76	5241	3051	no data	115	6263	−841
67	Proprietary data	10.27	−7.66	5323	3160	no data	119	6408	−949
68	Proprietary data	10.35	−7.96	5203	2907	no data	119	6122	−661
69	Proprietary data	10.35	−8.24	5371	2224	no data	119	5723	−264
70	Proprietary data	10.36	−8.56	5170	2602	no data	119	5863	−405
71	Proprietary data	10.38	−8.97	5475	2030	2080	119	5625	−167
72	*Cunningham et al.* [2002]	278.99	−68.05	5163	2003	no data	25	5398	−1073
73	*Cunningham et al.* [2002]	269.73	−69.68	5106	1862	no data	81	5246	354
74	Proprietary data	2.15	3.66	5467	3249	no data	94	6584	−1040
74	Proprietary data	2.80	3.19	5520	2769	no data	90	6254	−664
75	Proprietary data	3.16	3.45	5313	3053	no data	92	6318	−750
76	*Cunningham et al.* [2002]	270.95	−69.32	4891	1956	2183	34	5194	−580
77	*Cunningham et al.* [2002]	266.02	−69.47	4996	1959	1700	99	4977	496
77	*Cunningham et al.* [2002]	267.63	−69.49	5514	1746	1837	101	5287	163
78	*Cunningham et al.* [2002]	264.19	−69.44	5848	1997	1507	97	5525	−23
79	*Cunningham et al.* [2002]	263.19	−69.94	5715	2629	1709	98	6034	−546
80	*Cunningham et al.* [2002]	266.16	−69.79	4709	2352	1544	101	4965	488
81	*Beslier et al.* [1993]	346.97	40.66	7178	1451	no data	125	6487	−958
82	*Bunce and Molnar* [1977]	50.93	3.08	6478	820	no data	86	5481	130
82	*Bunce and Molnar* [1977]	51.42	2.25	6846	962	no data	61	5865	−661
83	*Bunce and Molnar* [1977]	51.38	3.90	6900	1473	no data	76	6295	−764
84	Proprietary data	8.11	0.76	3223	3139	no data	116	4816	609
85	Proprietary data	6.89	0.98	3819	3230	no data	107	5334	69
85	Proprietary data	7.54	0.30	3787	3086	no data	112	5198	206
86	Proprietary data	7.31	2.57	3399	3062	no data	104	4889	534
86	Proprietary data	7.43	2.44	3425	3124	no data	106	4956	454
86	Proprietary data	7.87	2.02	3359	3231	no data	113	4989	416
87	Proprietary data	7.33	2.57	3351	2752	no data	104	4614	807
87	Proprietary data	6.83	1.94	3975	2213	no data	105	4667	747
88	*Canales et al.* [2002]	265.62	2.69	3451	0	2106	1	2579	380
89	*Canales et al.* [2002]	268.39	2.28	3142	0	2448	1	2559	402
90	Proprietary data	312.93	3.57	3004	5697	no data	102	6643	−1207
91	*Collier et al.* [2009]	56.74	−3.17	5030	1001	1930	61	4415	782
92	*Collier et al.* [1998]	339.14	27.98	6260	1201	2774	135	6011	−381
93	*Collier et al.* [1998]	339.13	27.96	6231	1576	2559	135	6142	−512
94	*Collier and Watts* [2001]	344.41	29.79	4562	2512	no data	158	5337	364
95	*Collier and Watts* [2001]	344.46	28.67	4820	3194	no data	166	6057	−345
96	*Collier and Watts* [2001]	343.68	26.95	4766	3140	no data	167	5974	−263
97	*Collier and Watts* [2001]	343.52	27.51	4696	3033	no data	164	5840	−131
97	*Collier and Watts* [2001]	343.70	27.40	4664	3335	no data	165	6049	−338
98	*Collier and Watts* [2001]	343.18	27.08	4807	2801	no data	163	5744	−36
99	*Collier and Watts* [2001]	342.94	27.62	4781	2612	no data	160	5579	125
99	*Collier and Watts* [2001]	342.17	26.49	4778	1925	no data	161	5049	657
99	*Collier and Watts* [2001]	342.68	27.24	4842	2343	no data	160	5417	287
100	*Cooper et al.* [1992]	182.04	54.96	3803	4575	no data	68	6366	−996
100	*Cooper et al.* [1992]	183.76	55.86	3801	4125	no data	69	6014	−610
101	Proprietary data	85.38	15.84	3839	4700	1750	112	6250	−848
102	Proprietary data	86.60	16.14	3643	4485	2253	111	6247	−848
103	Proprietary data	86.76	16.50	3533	4677	2268	112	6323	−922
104	Proprietary data	86.71	17.74	3326	4769	2584	114	6434	−1022
104	Proprietary data	87.10	17.07	3360	5198	2064	112	6471	−1069
105	Proprietary data	87.30	17.73	3171	5677	1878	113	6589	−1184
105	Proprietary data	87.47	17.45	3213	5656	1880	112	6605	−1204

Table 1. (continued)

Profile	Reference	Longitude	Latitude	T_w, ms	T_s, ms	T_c, ms	Age, Ma	Z_{wl}, m	Z_{res}, m
105	Proprietary data	87.67	17.12	3299	5480	2057	110	6642	−1243
106	Proprietary data	87.80	17.82	3068	5987	1839	111	6729	−1329
106	Proprietary data	88.14	17.20	3294	5524	2102	109	6699	−1301
107	Proprietary data	88.10	18.20	3023	6073	1923	111	6815	−1415
107	Proprietary data	88.59	17.24	3233	5422	2293	108	6693	−1293
108	Proprietary data	88.33	18.68	2802	6286	1863	111	6778	−1378
109	Proprietary data	89.13	18.86	2430	6185	3201	110	7246	−1848
110	Proprietary data	88.66	17.91	2901	5780	2716	109	6984	−1585
110	Proprietary data	87.43	17.26	3310	5581	1941	111	6656	−1256
110	Proprietary data	87.69	17.39	3218	5700	1964	111	6695	−1295
111	Proprietary data	86.86	16.86	3444	4864	2196	112	6357	−954
112	Proprietary data	81.91	13.68	4438	3854	1697	115	6012	−593
113	Unpublished	304.00	−56.63	4373	0	2100	7	3268	277
114	Unpublished	302.15	−56.23	5108	0	2100	10	3819	−138
114	Unpublished	302.72	−56.35	4374	0	2100	9	3268	352
115	*Franke et al.* [2007]	309.58	−36.98	5931	2802	2175	120	6617	−1155
116	*Franke et al.* [2007]	303.44	−47.01	6127	2714	1517	128	6290	−731
117	*Franke et al.* [2007]	303.17	−43.98	6248	2374	2267	131	6583	−990
118	*Franke et al.* [2007]	304.96	−42.96	6255	2478	2452	124	6782	−1266
119	*Franke et al.* [2007]	303.80	−42.23	6767	2058	2188	133	6682	−1074
120	*Franke et al.* [2007]	304.79	−41.65	6165	2697	2207	130	6731	−1152
121	*Franke et al.* [2007]	306.60	−39.83	6451	2351	1904	125	6494	−966
122	*Franke et al.* [2007]	307.05	−38.42	5557	3412	no data	130	6778	−1196
123	*Gardner* [1970]	153.74	−14.83	6096	1041	no data	53	5362	−341
124	*Stagg et al.* [2004b]	46.85	−61.73	6417	1470	no data	120	5930	−464
124	*Stagg et al.* [2004b]	46.79	−62.94	5461	2407	no data	125	5930	−403
125	*Stagg et al.* [2004b]	52.41	−63.46	6256	2202	1437	130	5945	−366
125	*Stagg et al.* [2004b]	52.52	−63.32	6366	2035	1465	129	5917	−345
126	*Stagg et al.* [2004b]	56.84	−63.42	6294	1661	no data	129	5983	−408
127	*Stagg et al.* [2004b]	63.71	−62.33	5827	1505	2305	128	5628	−70
127	*Stagg et al.* [2004b]	63.74	−63.09	5651	2019	2046	129	5728	−151
128	*Stagg et al.* [2004b]	67.22	−62.26	5831	1724	2242	129	5758	−191
128	*Stagg et al.* [2004b]	67.27	−63.24	5505	2203	2123	130	5806	−220
129	*Stagg et al.* [2004b]	70.51	−62.06	5499	1588	2755	127	5723	−167
129	*Stagg et al.* [2004b]	70.54	−63.11	5268	2298	2195	130	5746	−165
130	*Stagg et al.* [2004b]	73.94	−63.43	5175	2294	2626	130	5939	−361
131	*Stagg et al.* [2004b]	90.55	−62.05	5356	1686	2732	125	5676	−155
131	*Stagg et al.* [2004b]	91.27	−62.90	5144	2537	2156	126	5812	−274
132	*Stagg et al.* [2004b]	97.34	−62.40	5415	1803	2974	129	5959	−385
132	*Stagg et al.* [2004b]	97.35	−62.58	5300	1768	2968	130	5842	−261
133	*Stagg et al.* [2004b]	100.71	−61.74	5958	1808	2469	126	6058	−517
134	*Stagg et al.* [2004b]	117.47	−61.28	5775	1814	1919	40	5585	−835
135	*Stagg et al.* [2004b]	126.06	−61.78	5843	2171	no data	53	6036	−1015
135	*Stagg et al.* [2004b]	126.11	−62.55	5644	2408	no data	72	6069	−609
136	*Stagg et al.* [2004b]	132.54	−61.10	6100	1791	2080	43	5911	−1088
137	*Stagg et al.* [2004b]	147.33	−63.09	5288	726	no data	36	4516	145
138	*Stagg et al.* [2004b]	153.80	−64.39	4706	1120	2042	23	4330	−66
139	*Stagg et al.* [2004b]	141.81	−61.90	5681	1120	no data	45	5112	−250
140	*Stagg et al.* [2004b]	112.23	−61.22	5692	1539	no data	39	5439	−714
141	*Stagg et al.* [2004b]	107.25	61.59	5779	1122	no data	40	5186	−445
142	*Stagg et al.* [2004b]	91.85	−61.06	5686	2170	2155	125	5936	−413
142	*Stagg et al.* [2004b]	93.13	−61.86	5441	2537	2008	126	5942	−406
143	*Stagg et al.* [2004b]	92.76	−61.12	5720	2384	1992	124	6025	−507
144	*Stagg et al.* [2004b]	91.05	−61.53	5585	1919	2549	124	5912	−400
144	*Stagg et al.* [2004b]	92.65	−61.80	5550	2302	2266	126	6004	−470
145	*Stagg et al.* [2004b]	75.76	−63.19	5110	1966	2787	128	5739	−174
146	*Stagg et al.* [2004b]	72.11	−62.48	5362	1931	3061	127	6070	−517
146	*Stagg et al.* [2004b]	72.16	−63.34	5162	2419	2391	129	5880	−310
147	*Stagg et al.* [2004b]	68.71	−62.28	5638	1920	2004	129	5616	−45
147	*Stagg et al.* [2004b]	68.73	−63.21	5277	2445	1973	131	5728	−140
148	*Stagg et al.* [2004b]	65.59	−62.31	5870	1690	2377	128	5845	−282
148	*Stagg et al.* [2004b]	65.52	−63.18	5592	2079	2243	130	5851	−268

Table 1. (continued)

Profile	Reference	Longitude	Latitude	T_w, ms	T_s, ms	T_c, ms	Age, Ma	Z_{wl}, m	Z_{res}, m
149	*Stagg et al.* [2004b]	61.66	−62.42	6109	1188	2537	128	5741	−175
149	*Stagg et al.* [2004b]	62.11	−63.08	5860	1752	2169	129	5757	−184
149	*Stagg et al.* [2004b]	62.52	−63.68	5375	2078	2712	132	5976	−379
150	*Stagg et al.* [2004b]	60.59	−63.67	6088	1566	2148	132	5772	−172
151	*Stagg et al.* [2004b]	41.09	−63.84	6517	1543	no data	124	6061	−546
152	*Stagg et al.* [2004b]	54.84	−62.33	6682	1532	1570	126	5835	−300
152	*Stagg et al.* [2004b]	53.36	−63.05	6475	1954	1481	128	5947	−389
155	*Dean et al.* [2000]	346.93	40.45	6957	1736	1968	125	6443	−921
156	*Rebesco et al.* [1996]	284.07	−66.75	4722	1483	no data	22	4669	−449
156	*Rebesco et al.* [1996]	282.45	−67.98	5016	1570	no data	24	4956	−668
156	*Rebesco et al.* [1996]	282.80	−67.72	4583	1874	no data	22	4864	−629
157	Proprietary data	42.94	−4.64	5226	3133	1593	145	5983	−305
158	Proprietary data	43.46	−3.40	5026	3378	1640	150	6050	−361
159	*Lau et al.* [2006]	313.11	43.50	5873	2369	2090	123	6189	−687
160	*Lau et al.* [2006]	314.40	44.76	5202	2108	no data	120	5507	−41
161	*Lau et al.* [2006]	314.28	44.59	5259	1671	no data	120	5215	255
162	*Lau et al.* [2006]	313.96	44.23	5710	1766	1451	122	5211	274
163	*Lucazeau et al.* [2008]	54.27	16.23	3640	1018	no data	21	3503	694
164	*McBride et al.* [1994]	337.08	24.07	6432	1293	no data	138	5806	−157
165	*McBride et al.* [1994]	336.96	24.14	6537	1331	1256	137	5380	263
166	*McBride et al.* [1994]	337.06	24.08	6421	1083	no data	138	5638	11
167	*McBride et al.* [1994]	337.19	24.02	6700	1165	no data	139	5909	−254
167	*McBride et al.* [1994]	337.52	23.95	6749	1248	no data	143	6009	−339
168	Proprietary data	46.51	−13.06	4570	2842	2074	152	5564	128
169	Proprietary data	45.68	−13.79	4555	3208	2461	151	6074	−382
170	Proprietary data	44.87	−13.73	4680	3141	2082	147	5882	−199
171	Proprietary data	44.16	−13.94	4672	3122	2192	148	5929	−244
172	Proprietary data	50.45	−11.56	5264	889	no data	94	4622	919
173	*Miles et al.* [1998]	64.44	15.13	3383	3665	no data	55	5343	−263
174	*Miles et al.* [1998]	63.95	15.02	3487	3113	no data	55	4995	76
175	*Miles et al.* [1998]	65.07	15.04	3785	2820	no data	55	4992	89
177	*Thinon et al.* [2003]	352.22	46.04	6482	1794	1428	94	5798	−258
177	*Thinon et al.* [2003]	352.58	46.45	6373	3367	40	100	6064	−601
178	*Ranero et al.* [2003]	254.58	16.09	3794	0	1865	0	2688	−50
179	*Ranero et al.* [2003]	273.69	10.18	5331	480	no data	23	4362	−84
180	*Ranero et al.* [2003]	273.43	10.41	5512	593	1618	25	4273	60
181	*Ranero et al.* [1997]	152.64	36.40	7749	340	2234	136	6140	−509
182	*Ranero et al.* [1997]	150.65	40.41	7062	484	2178	127	5699	−145
183	*Ranero et al.* [1997]	150.96	39.74	7143	486	2053	129	5684	−116
184	*Rodger et al.* [2006]	313.38	5.39	4749	3262	no data	81	6056	−454
185	*Geoscience Australia* [2008]	113.73	−32.41	5862	1059	2176	126	5234	303
187	*Sage et al.* [2000]	357.24	2.91	6658	1802	no data	80	6365	−778
188	*Ball* [2005]	140.75	−61.53	5809	826	no data	51	4983	7
189	Proprietary data	56.45	−2.92	5665	873	1446	61	4494	709
190	Proprietary data	56.27	−3.21	5288	943	1735	61	4444	771
191	*Hopper et al.* [2003]	322.40	62.71	2788	1414	4344	52	4538	470
191	*Hopper et al.* [2003]	322.77	62.59	2886	1318	3943	51	4291	698
191	*Hopper et al.* [2003]	323.69	62.29	3459	1195	3273	49	4213	729
192	Proprietary data	66.92	19.93	4384	2665	1901	79	5182	399
193	Proprietary data	321.86	−22.01	4675	1967	2149	113	5019	386
194	Proprietary data	321.98	−22.14	4649	1940	no data	112	4963	441
195	Proprietary data	314.31	−28.15	3696	3632	no data	119	5553	−93
196	Proprietary data	313.99	−28.20	3436	3886	no data	119	5554	−94
197	Proprietary data	314.15	−28.16	3595	3677	2589	119	5793	−335
198	Proprietary data	314.36	−27.90	3563	3694	2713	119	5859	−398
199	Proprietary data	314.32	−27.36	2984	3856	3042	120	5753	−290
199	Proprietary data	314.52	−27.71	3496	3978	2023	119	5603	−144
200	Proprietary data	314.41	−27.36	3135	3970	no data	119	5394	67
200	Proprietary data	314.69	−27.83	3831	3679	no data	118	5690	−241
201	Proprietary data	314.77	−27.34	3467	3944	no data	119	5623	−167
201	Proprietary data	314.93	−27.62	3693	3908	no data	118	5764	−314
202	Proprietary data	321.40	−22.48	4218	2008	2143	114	4705	706

Table 1. (continued)

Profile	Reference	Longitude	Latitude	T_w, ms	T_s, ms	T_c, ms	Age, Ma	Z_{wl}, m	Z_{res}, m
202	Proprietary data	321.64	−22.58	4447	2078	2144	112	4930	474
203	Proprietary data	321.60	−22.41	4454	2160	no data	113	4986	421
203	Proprietary data	321.90	−22.52	4938	1424	no data	112	4786	616
204	Proprietary data	321.84	−22.26	4534	1992	2119	112	4914	489
205	Proprietary data	321.74	−22.07	4595	1716	no data	113	4751	657
206	Proprietary data	321.76	−21.96	4612	1858	2453	113	5077	332
207	Proprietary data	321.75	−21.84	4644	2041	2302	114	5147	264
208	Proprietary data	321.77	−21.77	4684	1963	2352	114	5148	263
209	Proprietary data	321.77	−21.61	4715	1954	2262	114	5109	303
210	Proprietary data	321.82	−21.52	4724	2150	2226	114	5244	167
211	Proprietary data	321.57	−21.73	4487	2111	2537	115	5229	191
212	Proprietary data	321.76	−21.68	4646	1958	2473	114	5191	220
213	Proprietary data	321.83	−21.90	4663	1938	2315	113	5091	317
214	*Thinon et al.* [2003]	352.44	45.57	6428	1386	no data	88	5874	−271
214	*Thinon et al.* [2003]	352.81	46.13	6210	2283	no data	96	6397	−887
215	*Tsuji et al.* [2007]	146.83	27.15	7375	516	2245	148	5999	−315
215	*Tsuji et al.* [2007]	147.85	27.07	7736	360	1999	150	6000	−311
216	*Tsuji et al.* [2007]	146.14	25.18	7510	1006	1910	147	6265	−582
217	*Tsuji et al.* [2007]	147.12	27.59	7557	453	2029	148	5955	−270
217	*Tsuji et al.* [2007]	147.07	27.16	7362	393	2408	148	5998	−312
218	*Tucholke et al.* [2007]	347.36	40.85	6959	1542	no data	129	6391	−824
221	Proprietary data	42.97	−8.25	5005	2789	2012	122	5811	−318
222	Proprietary data	43.31	−7.38	5324	2216	2099	129	5666	−96
223	Proprietary data	43.67	−4.71	5623	2519	1615	144	5823	−148
224	Proprietary data	68.06	18.25	4453	2625	1637	78	5041	528
226	Proprietary data	70.61	15.20	5173	1452	2097	59	4968	187
227	*Moulin et al.* [2005]	10.18	−8.05	5411	2650	1877	119	5926	−474

where $\rho_w = 1$ Mg m^{-3} and $\rho_s = 2.65$ Mg m^{-3} are the densities of water and solid sediment, respectively.

To determine the water-loaded subsidence of oceanic floor, a sedimentary column is replaced with an equivalent column of water, S_w, which is added to the water depth, d_w.

$$S_w = \left(\frac{\rho_a - \bar{\rho}}{\rho_a - \rho_w}\right) z + d_w, \tag{6}$$

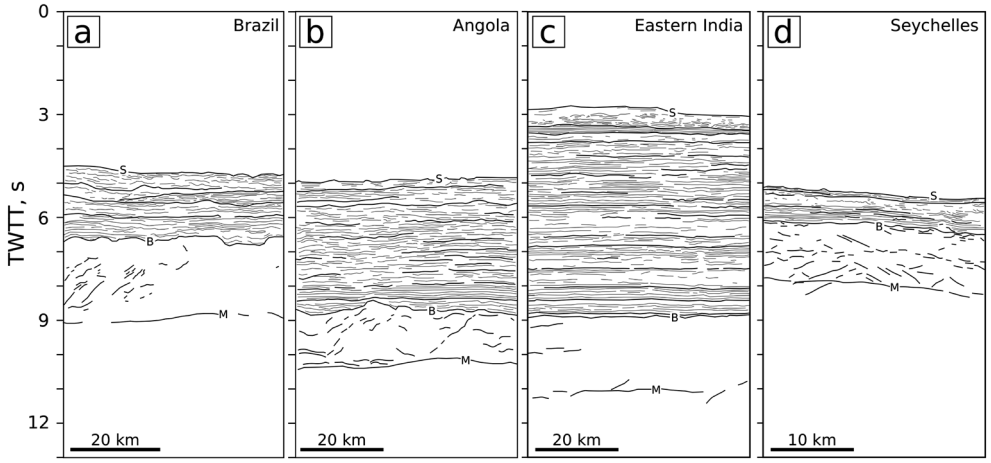

Figure 2. Detailed line drawings of seismic reflection profiles from old, thickly sedimented oceanic crust that abuts continental margins. S = seabed; B = sediment-basement interface; M = base of crust (Moho). Internal layering of sedimentary column and structure of oceanic crust are shown. (a) Offshore Brazilian margin: thin sediment and average crustal thickness; (b) offshore Angolan margin: thick sediment and anomalously thin crust; (c) offshore East Indian margin: very thick sediment and average crustal thickness; (d) offshore Seychelles Islands: thin sediment and thin crust.

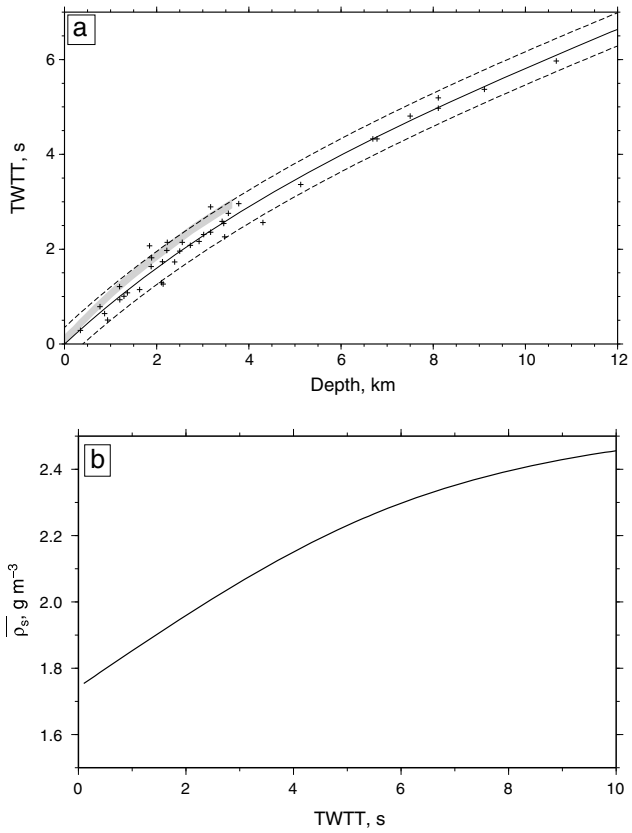

Figure 3. (a) Empirical relationship between two-way travel time and depth for sedimentary columns beneath the oceans. Crosses = measurements from global data set of coincident seismic reflection and wide-angle surveys [see *Winterbourne et al.*, 2009, Table 2]; solid line = best fitting relationship, which assumes that acoustic velocity is function of sediment porosity; dashed lines = error bounds [*Winterbourne et al.*, 2009]; gray band = relationship of *Tucholke et al.* [1982]. (b) Variation of density as function of two-way travel time derived using values of initial porosity and compaction decay length estimated from Figure 3a.

where $\rho_a = 3.2$ Mg m^{-3} is the density of the asthenosphere. If crustal thickness differs from the global average of 7.1 km [*White et al.*, 1992], a smaller isostatic correction, C_w, is made such that

$$C_w = \left(\frac{\rho_a - \rho_c}{\rho_a - \rho_w}\right)(t_c - 7.1), \qquad (7)$$

where t_c and $\rho_c = 2.8$ Mg m^{-3} are the measured thickness of oceanic crust and its density.

Four interpreted images of oceanic crust are shown in Figure 2. We use these examples to illustrate the importance of accurately correcting for sediment and crustal loading. For example, the Brazilian and Angolan margins have near-identical water depths of 3.4 km. Using the relationships shown in Figure 3, we find that the sedimentary thicknesses and average densities are 2.5 ± 0.25 km and 2.0 Mg m^{-3} for Brazil and 6 ± 0.3 km and 2.2 Mg m^{-3} for Angola. These values yield water-loaded subsidence values of 4.8 ± 0.14 and 6.1 ± 0.14 km, respectively. The average crustal thickness beneath the Brazilian margin is 8.4 km and beneath the Angolan margin is 5.0 km. This difference yields isostatic corrections of +0.3 and −0.4 km, respectively. The water-loaded subsidence at each margin is 5.1 ± 0.2 and 5.7 ± 0.2 km. Similarly, offshore Eastern India has a shallower water depth of 2.3 km but its water-loaded subsidence is nearly 7 km. The size of these corrections emphasizes the importance of accurate measurements of sedimentary and crustal thicknesses.

In Figure 4a, the residual depth is the vertical distance from the calculated water-loaded subsidence to the age-depth relationship. Offshore Brazil has a small residual depth of +0.25 km, whereas offshore Angola has a residual depth of −0.8 km. Eastern India has the largest negative residual depth of −1.4 km, and the Seychelles is +0.5 km. By carefully propagating uncertainties at each stage of these calculations, *Czarnota et al.* [2013] showed that residual depth measurements are well resolved with typical uncertainties of ±100 m. These uncertainties grow with increasing sedimentary thickness. Our measurements of water-loaded subsidence are shown in Figure 4b. Residual depth anomalies exist for plate ages of 0 to 180 Ma, and their amplitudes rarely exceed ±1 km. We infer that the amplitude of dynamic topography in the strict sense is some fraction of this range of amplitudes.

4. Spatial Distribution of Residual Topography

Residual depth measurements, averaged over 2° × 2° cells (10° × 2° above 82°N and below 82°S), were used to construct a set of global maps (Figure 5). These maps were augmented with residual depth measurements from a 5 Ma wide strip along active and fossil mid-oceanic ridges, not all of which were analyzed by *Müller et al.* [2008]. We also included a carefully chosen network of ship track bathymetric profiles where sediment thickness is less than 1500 m. Oceanic plateaux and other areas with thickened oceanic crust were

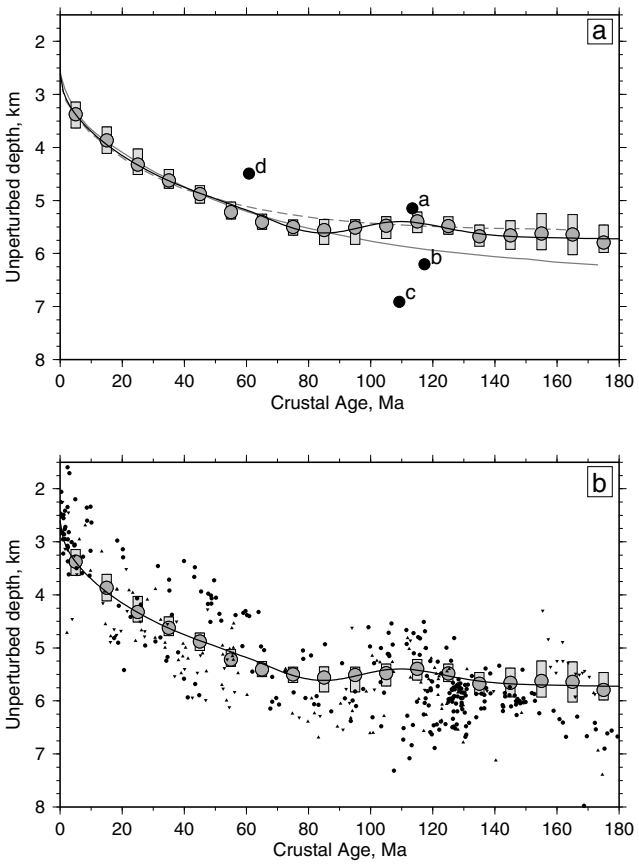

Figure 4. Age-depth relationships. (a) Gray circles, error bars, and thin black line = age-depth relationship from *Crosby et al.* [2006]; solid circles labeled a–d = water-loaded subsidence of oceanic crust determined from seismic reflection profiles shown in Figure 2; gray line = age-depth relationship of *Parsons and Sclater* [1977]; dashed line = age-depth relationship of *Stein and Stein* [1992]. In each case, vertical distance from age-depth curve is residual depth anomaly (i.e., dynamical topography). (b) Measurements of 449 of water-loaded subsidence of oceanic crust.

excised by eye, following the polygons of *Crosby and McKenzie* [2009]. In the North Atlantic Ocean, we have corrected for thickened crust in the vicinity of the Icelandic plume [*Jones et al.*, 2002].

Many well-known features are visible on these maps. The Northern Hemisphere is dominated by the Icelandic plume, which has a positive residual topography of 1–2 km. It reaches from Baffin Bay to western Norway, and from north of the Azores to Svalbard. South of Iceland, residual topography is asymmetric: the Iceland basin to the west has a larger residual depth anomaly than the Irminger basin to the east. The northernmost part of Baffin Bay and the bulk of the Arctic Ocean, including the Gakkel Ridge and the Beaufort Sea, have negative residual topographic anomalies. Substantial anomalies occur in the Gulf of Mexico, in the southern Caspian Sea, and in the Red Sea.

In the Southern Hemisphere, prominent residual depth anomalies occur in the Argentine abyssal plain, in the Pacific and Southern Oceans, in Southeast Asia, and between Australia and Antarctica. *Hayes* [1988] and *Marty and Cazenave* [1989] both showed that the Argentine abyssal plain is anomalously deep given its plate age. *Hohertz and Carlson* [1998] suggested that this anomaly invalidated the plate-cooling model. It is more likely that this region is convectively drawn downward.

Nyblade and Robinson [1994] showed that a region encompassing subequatorial Africa and a large portion of oceanic floor is anomalously elevated by 500 m. Our measurements confirm the existence of this Southern Ocean superswell but reveal that it has an irregular outline with short-wavelength excursions. For example, there is a shorter-wavelength variation of residual depth along the West African coastline, which intersects the coastline [*Al-Hajri et al.*, 2009]. Off southern Africa, Madagascar perches on the northwest edge of a protruding tongue of positive residual topography, which might account for its asymmetric physiography [*Roberts et al.*, 2012]. Further north, the East Somali basin is drawn down by ~350 m. The west coast of India has positive residual topography, but the east coast has a large negative residual anomaly [*Becker and Faccenna*, 2011]. This steep gradient may account for the asymmetric topography of the subcontinent which is probably of Neogene age.

Between Australia and Antarctica, there is excellent evidence for large-scale negative residual topography, and it has been previously suggested that this Australian-Antarctic Discordance is supported by cold downwelling mantle [see *Holmes et al.*, 2010, and references therein]. *Whittaker et al.* [2010] used the same set of conjugate reflection profiles to estimate residual topography along the margins of South Australia and Antarctica. Their sedimentary correction differs from that exploited here, they do not explicitly correct for crustal thickness, and they used a different age-depth relationship. Nonetheless, there are important

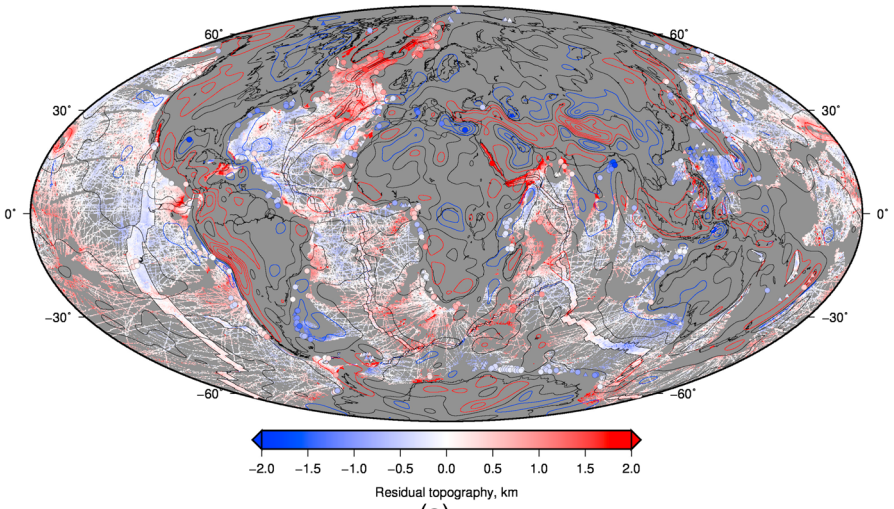

(a)

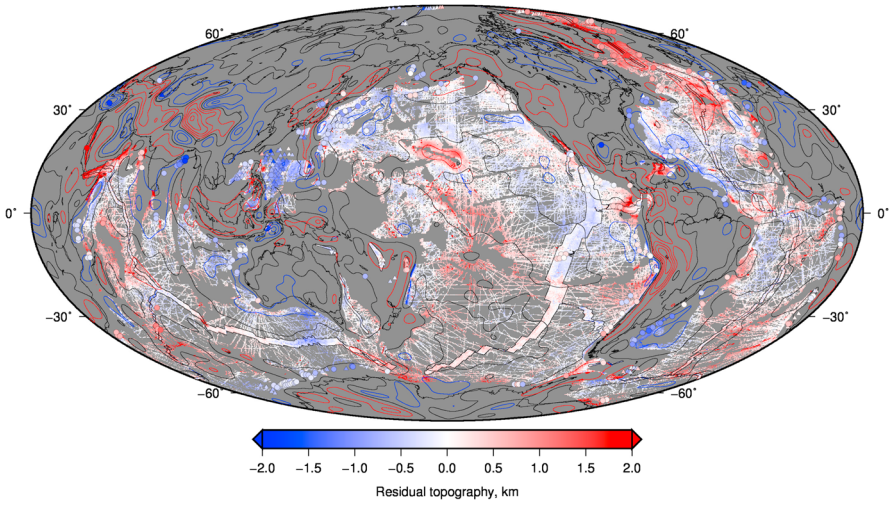

(b)

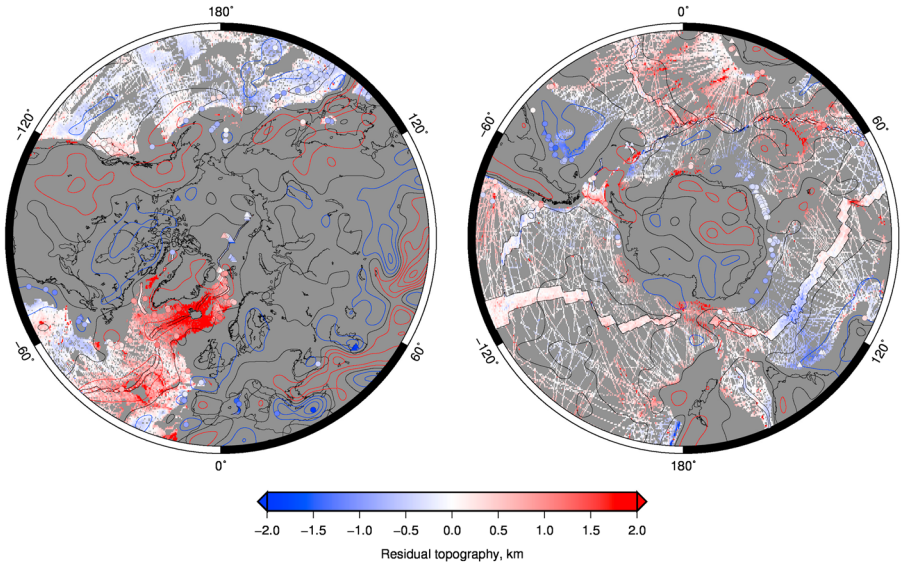

(c)

Figure 5.

similarities. The most significant difference is that our residual depth anomalies on the Antarctic margin are larger.

Negative residual depth anomalies occur throughout southeast Asia, stretching from the northern margin of Australia to the Sea of Okhotsk and from the Andaman Sea to the Marianas Arc. These anomalies were mainly determined by analyzing the age-depth relationships of numerous fragments of oceanic crust [*Wheeler and White*, 2000]. The average residual depth is −500 m. Observations from Southeast Asia are of particular importance since most dynamic models predict that this region is the largest drawn-down region on Earth [e.g., *Flament et al.*, 2013].

5. Transects and Correlations

It is helpful to examine empirically the correlation between global residual depth anomalies, free-air gravity anomalies, and seismic tomographic models. The quality of these correlations enables us to assess the extent to which present-day residual depth anomalies are generated by convective circulation beneath the lithospheric plate. Long-wavelength (i.e., 800–2000 km) free-air gravity anomalies can be regarded as a crude proxy for subplate density anomalies. Shorter-wavelengths caused by flexural and edge effects at plate boundaries and continental margins have been removed. Longer wavelengths, which reflect the geoid, are also not considered here. In the oceans, dynamic topography in a broad sense can be estimated from these anomalies for an admittance value, $z = 30 \pm 10$ mgal km^{-1}, which is appropriate for wavelengths of greater than 800 km [e.g., *Crosby et al.*, 2006; *Crosby and McKenzie*, 2009]. Separately, surface wave and body wave tomographic models reveal the spatial pattern of velocity anomalies within the mantle which can be interpreted as temperature and density anomalies. By examining empirical correlations between these different data sets, we are ignoring the less tractable problem of how convective flow deforms the Earth's surface [*Flament et al.*, 2013].

In Figures 6–9, four transects are shown, along which residual depth, gravity, and tomographic anomalies can be compared. We have chosen vertical slices through the S40RTS tomographic model of *Ritsema et al.* [2011]. Similar results have been obtained using other global tomographic models (e.g., TXBW) [*Grand*, 2002]. The first transect runs north-south along the oldest oceanic floor on the western side of the Atlantic Ocean. There are 47 measurements of residual depth along this transect with amplitudes which range from +1 to −1.5 km. The steepest gradients (1:1000) occur across the Falkland Plateau and across the Nova Scotia margin. The middle portion of this transect is dominated by negative residual depths. Correlation between residual depth measurements and dynamic topography estimated from long-wavelength gravity anomalies is good, especially within the Argentine abyssal plain and within the Scotia Sea. The relationship between residual depth and tomographic anomalies is less clear. The best correlation occurs at the southern end of the transect where upper mantle velocities change from fast to slow from the Argentine abyssal plain toward the Scotia Sea. A steep gradient in residual depth from Nova Scotia to the Labrador Sea is matched by a similar pair of velocity anomalies in the middle of the upper mantle.

The second transect crosses remnants of oceanic lithosphere along the Tethyan collisional belt from the northwest shelf of Australia to offshore Newfoundland (Figure 7). Along this transect, residual topography

Figure 5. Global map of residual depth centered on Africa (Hammer Equal Area projection). Red colors = negative (i.e., shallow) residual depth; blue colors = positive (i.e., deep) residual depth. Filled circles = locations where sedimentary and crustal thicknesses are known with high degree of confidence and residual depth is accurate; upward pointing triangles = locations where regional evidence suggests that crustal thickness is thinner than average, which gives lower limit for residual depth; downward pointing triangles = locations where regional evidence suggests that crustal thickness is thicker than average, which gives upper limit for residual depth. Circles and triangles of 449 are spatially averaged onto 2° grid (at latitudes > 82°, they are averaged onto 2° latitude by 10° longitude grid). Network of irregular strips outlined in black = residual depth of active and fossil mid-oceanic ridge system; filigree (or spider's web) of ship tracks = residual depth of selected bathymetric profiles of *Smith and Sandwell* [1997] (areas of thick sediment and known oceanic plateaux were excised). Crustal thickness of 7.1 km was used in absence of independent constraints, a sediment thickness correction was applied using NGDC grid [*Divins*, 2008], and a depth-age correction was applied using oceanic age grid of *Müller et al.* [2008]. Red, black, and blue contours = positive, zero, and negative contours of filtered Gravity Recovery and Climate Experiment (GRACE) gravity anomaly [*Tapley et al.*, 2005] plotted every 20 mGal (∼1 km of dynamic topography). Global map of residual depth centered on Pacific Ocean (see previous page for details). Polar projections of residual depth (see previous page for details).

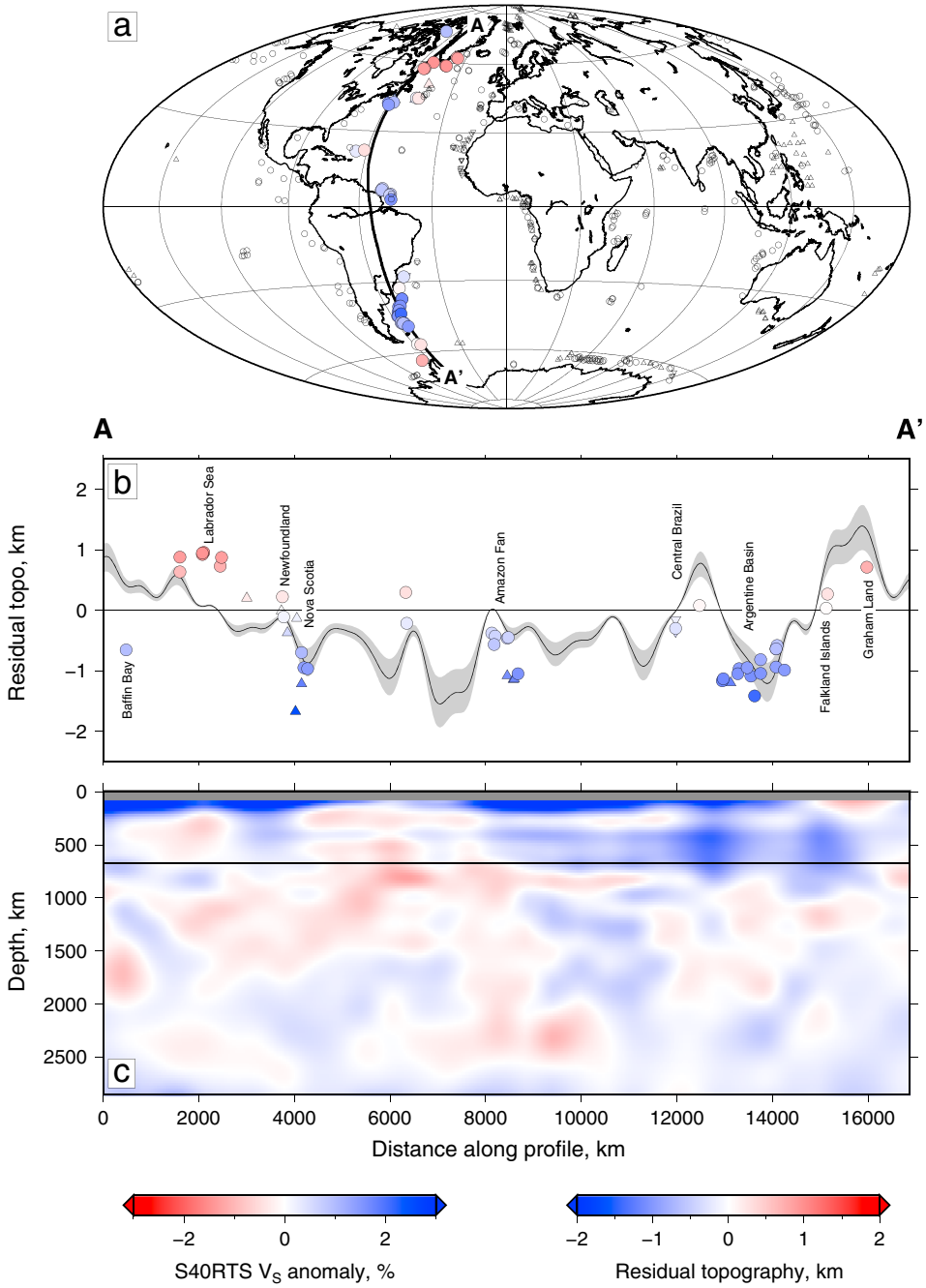

Figure 6. (a) Traverse, **A-A′**, showing variation of residual depth of oceanic crust from Baffin Bay to Antarctic Peninsula (Hammer Equal Area projection). Colored circles = estimates of residual depth made from oceanic crust (see Figures 5–7 and text); colored/open triangles and inverted triangles = lower and upper limits of residual depth; open circles and triangles = other estimates of residual depth. Note scale at bottom right-hand side. (b) Residual depth plotted as function of distance along **A-A′**. Circles and triangles as above; black line with gray band = residual depth predicted from long-wavelength free-air gravity anomaly, assuming $Z = 20–40$ mGal/km. (c) Vertical slice from S40RTS seismic tomographic model of *Ritsema et al.* [2011]. Note scale at bottom left-hand side. Horizontal line = 670 km discontinuity. Gray band marks top 100 km (i.e., lithosphere).

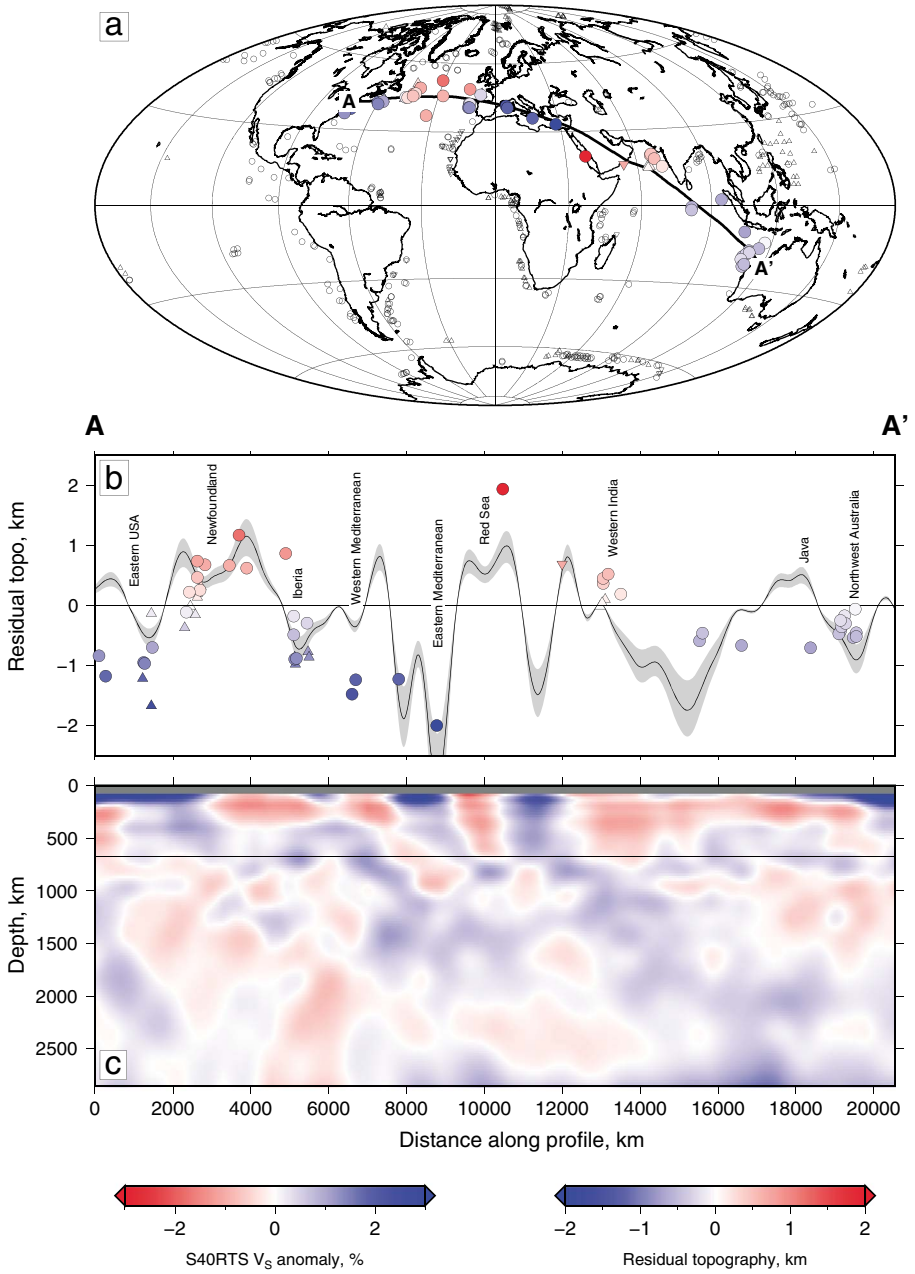

Figure 7. (a) Traverse, **A-A′**, showing variation of residual depth for oceanic crustal fragments from Northwestern Australia to East coast of North America (Hammer Equal Area projection). See Figure 6 for details. (b) Residual plotted as function of distance along **A-A′**. (c) Vertical slice from S40RTS seismic tomographic model.

varies dramatically on wavelengths as short as 500–1000 km. The steepest gradient occurs at the center of the transect between the Red Sea, which has a residual anomaly of almost +2 km and the east Mediterranean Sea which a residual anomaly of −2 km. There is also a large difference between the Iberian and Newfoundland margins. The positive residual depth anomaly associated with the Azorean plume is clearly visible between eastern North America and Iberia. As before, correlation between residual depth measurements and gravity anomalies is good, although it breaks down in the Indian Ocean. The Azorean plume, the Red Sea and western India are all associated with positive long-wavelength gravity anomalies, whereas the east coast of North America, the eastern Mediterranean Sea, and the northwest shelf of Australia have negative residual depths and gravity anomalies. Some of these anomalies are matched by upper mantle velocity anomalies. For example, there is a significant slow velocity anomaly associated with the Azorean plume. A slow velocity anomaly also occurs beneath the Red Sea.

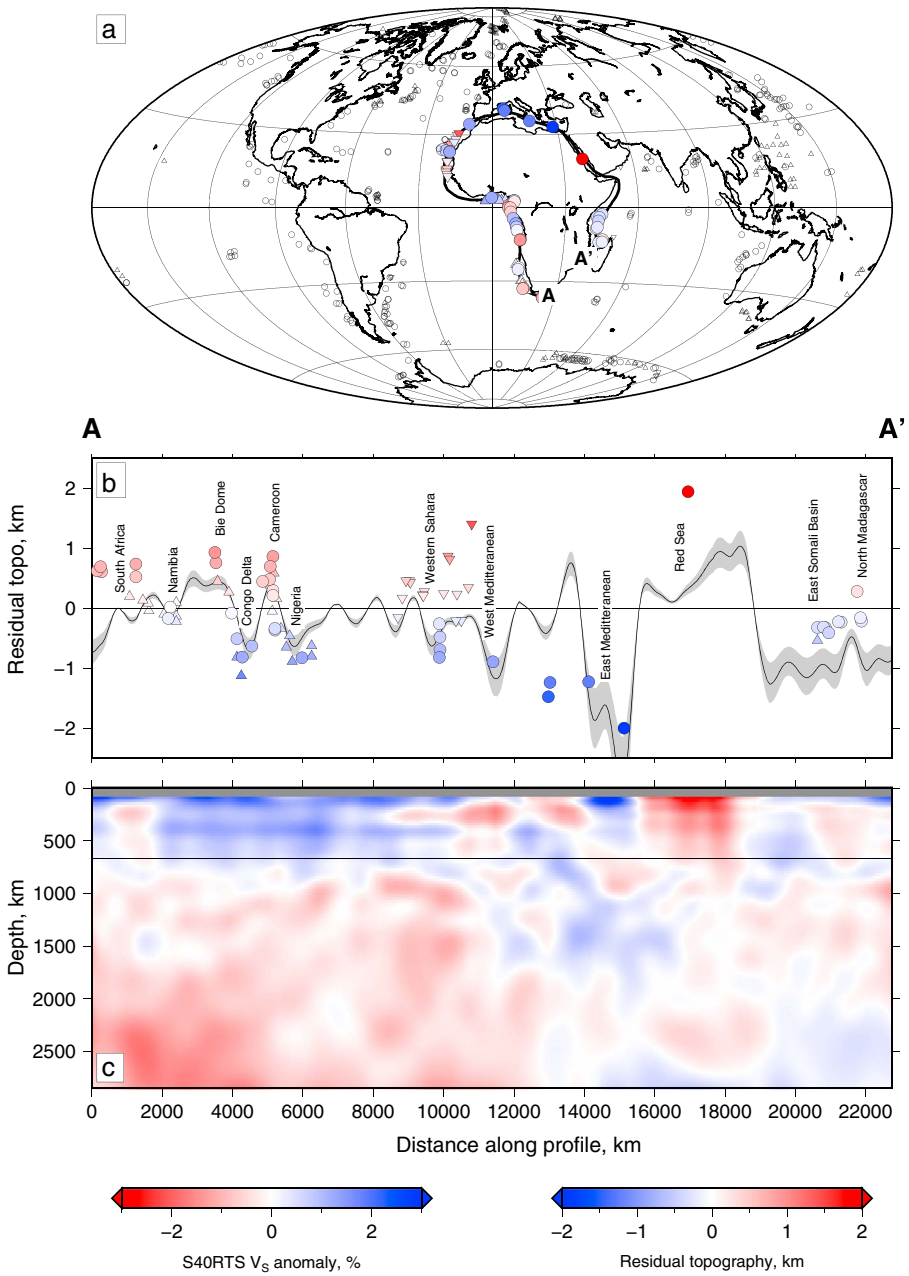

Figure 8. (a) Traverse, **A-A′**, encircling Africa which shows variation of residual depth for oceanic crust (Hammer Equal Area projection). See Figure 8 for details. (b) Residual depth plotted as function of distance along **A-A′**. (c) Vertical slice from S40RTS seismic tomographic model.

The third transect encircles the African continent (Figure 8). The best resolved portion of this transect is along the West African coastline where the oldest oceanic crust has well-resolved residual depth anomalies which vary between ±1 km with a wavelength of ~1800 km. Two prominent highs occur, the Bié Dome, which straddles the Angolan continental margin, and the Cameroon Line, which follows a chain of Cenozoic volcanism. Along the Mediterranean coastline, residual depth is increasingly negative, reaching −2 km in the eastern Mediterranean Sea. These variations are closely matched by long-wavelength gravity anomalies. The correlation between seismic tomographic anomalies and residual depth measurements is less clear. The most striking discrepancy occurs along the west coast of Africa where existing tomographic models do not resolve short-period variations. However, regional surface wave tomographic models do suggest

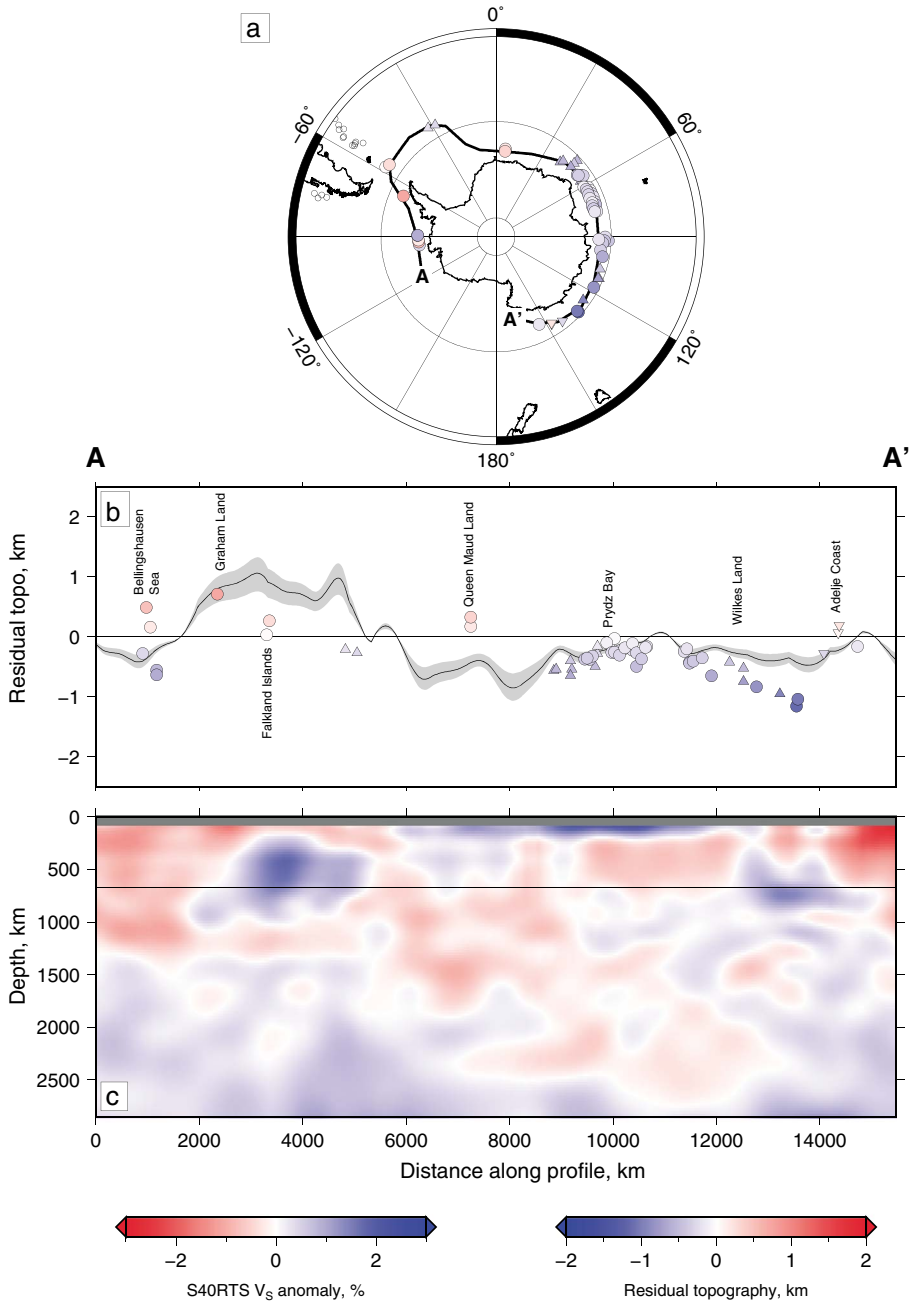

Figure 9. (a) Traverse, **A-A′**, encircling Antarctica which shows variation of residual depth for oceanic crust (Hammer Equal Area projection). See Figure 8 for details. (b) Residual depth plotted as function of distance along **A-A′**. (c) Vertical slice from S40RTS seismic tomographic model.

that the Bié dome and the Cameroon Line are underlain by slow velocity anomalies [*Al-Hajri et al.*, 2009; *Fishwick*, 2010].

A final transect encircles Antarctica (Figure 9). Away from the Ross Sea area, the fringes of this continent are dominated by negative residual depth anomalies. Long-wavelength gravity anomalies match these measurements reasonably well. The Australian-Antarctic Discordance has a prominent fast velocity anomaly within the top of the upper mantle. This anomaly disappears toward Adelje Land and is replaced by a large slow anomaly which fills the upper mantle and coincides with positive residual depth measurements. Further west, a thin layer of slow velocity anomalies within the upper mantle match positive residual depth measurements beneath the Scotia Sea.

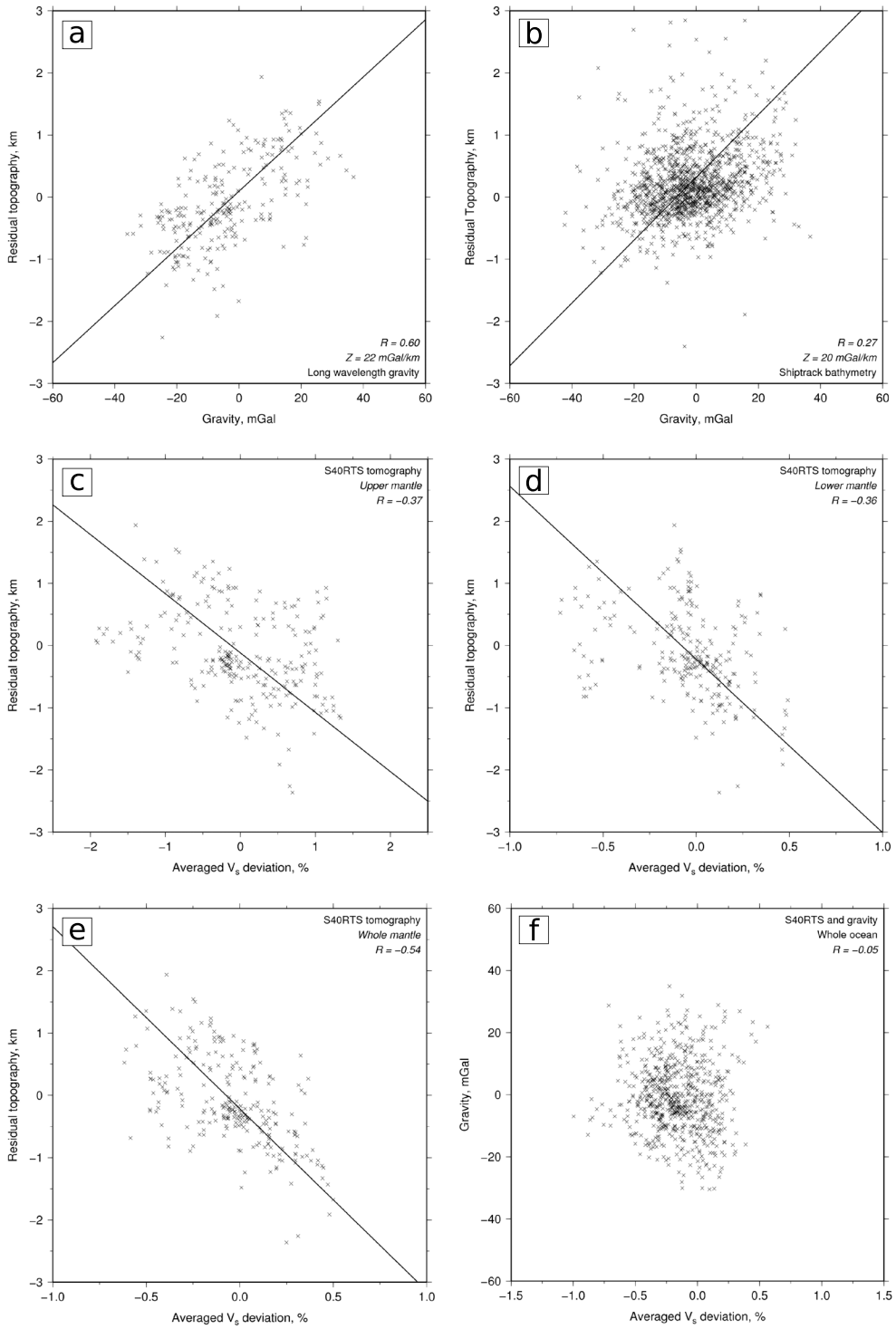

Figure 10. Relationships between spot measurements of residual topography where crustal thickness is known, free-air gravity anomalies and seismic tomographic anomalies. (a) Correlation between residual topography and long-wavelength free-air gravity anomalies (250 points). Optimal band-pass filter for gravity data is 700–12,400 km. (b) Correlation between residual topography measured from ship track bathymetry and long-wavelength gravity anomalies (1287 points). (c) Correlation between shear velocity anomalies averaged over upper mantle (100–675 km) and spot measurements of residual topography (250 points). (d) Correlation between shear velocity anomalies averaged over lower mantle (675–2850 km) and spot measurements of residual topography (250 points). (e) Correlation between shear velocity anomalies averaged over whole mantle (100–2850 km) and spot measurements of residual topography (250 points). (f) Correlation between shear velocity anomalies averaged over whole mantle and long-wavelength gravity anomalies (703 points).

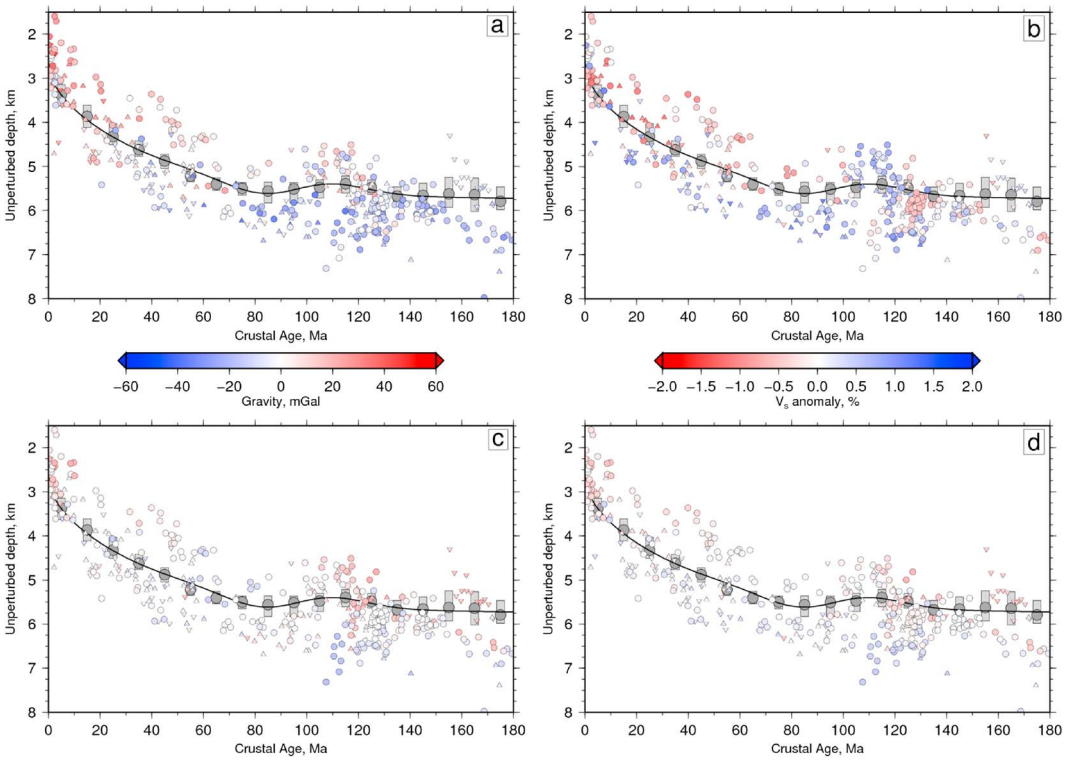

Figure 11. Residual depth measurements as function of plate age. (a) Gray circles, error bars and black line = age-depth relationship from *Crosby et al.* [2006]; red and blue circles and triangles = 449 global measurements of water-loaded subsidence of oceanic crust where color indicates amplitude of long-wavelength free-air gravity anomaly (see Figures 5–7). (b) As before but color indicates amplitude of shear velocity anomaly averaged over upper mantle (100–675 km). (c) As before but color indicates amplitude of shear velocity anomaly averaged over lower mantle (675–2850 km). (d) As before but color indicates amplitude of shear velocity anomaly averaged over whole mantle (100–2850 km).

A more formal analysis of the correlation between residual depth, gravity anomalies, and seismic tomographic models is presented in Figure 10. The strongest correlation is between a subset of 250 spot measurements of residual topography, for which sedimentary and crustal corrections can both be accurately determined, and gravity anomalies (Figure 10a). The correlation coefficient is 0.6 and the slope (i.e., the admittance) is $Z = 22$ mgal km^{-1}. This relationship suggests that many residual depth anomalies could be produced within the uppermost mantle [e.g., *Crosby and McKenzie*, 2009]. The quality of correlation is degraded when 1287 residual depth anomalies estimated from ship track bathymetric data are used instead (Figure 10b). In this case, the correlation coefficient decreases to 0.3, which suggests that residual measurements, for which sedimentary and crustal corrections are not accurately determined, should be treated with appropriate caution.

Correlations between residual depth measurements and velocity anomalies from the S40RTS tomographic model are shown in Figures 10c and 10d. In each case, we calculated the average velocity anomaly over a particular depth range (e.g., asthenosphere, upper mantle, and lower mantle). This empirical approach sidesteps the complicated and unresolved problem of converting velocities into densities or temperatures. It also ignores the effects of flow in the mantle. The average shear velocity anomaly, $\overline{\Delta V_s}$, is given by

$$\overline{\Delta V_s} = \frac{1}{N}\sum_{i=1}^{N} \Delta V_{s_i}, \tag{8}$$

where N is the number of layers in the sum and ΔV_{s_i} is the percentage shear velocity anomaly of the layer. We assume that

$$\Delta V_{s_i} = 100\left(\frac{V_s^{\mathrm{obs}}(Z)}{V_s^{\mathrm{ref}}(Z)}\right) - 100. \tag{9}$$

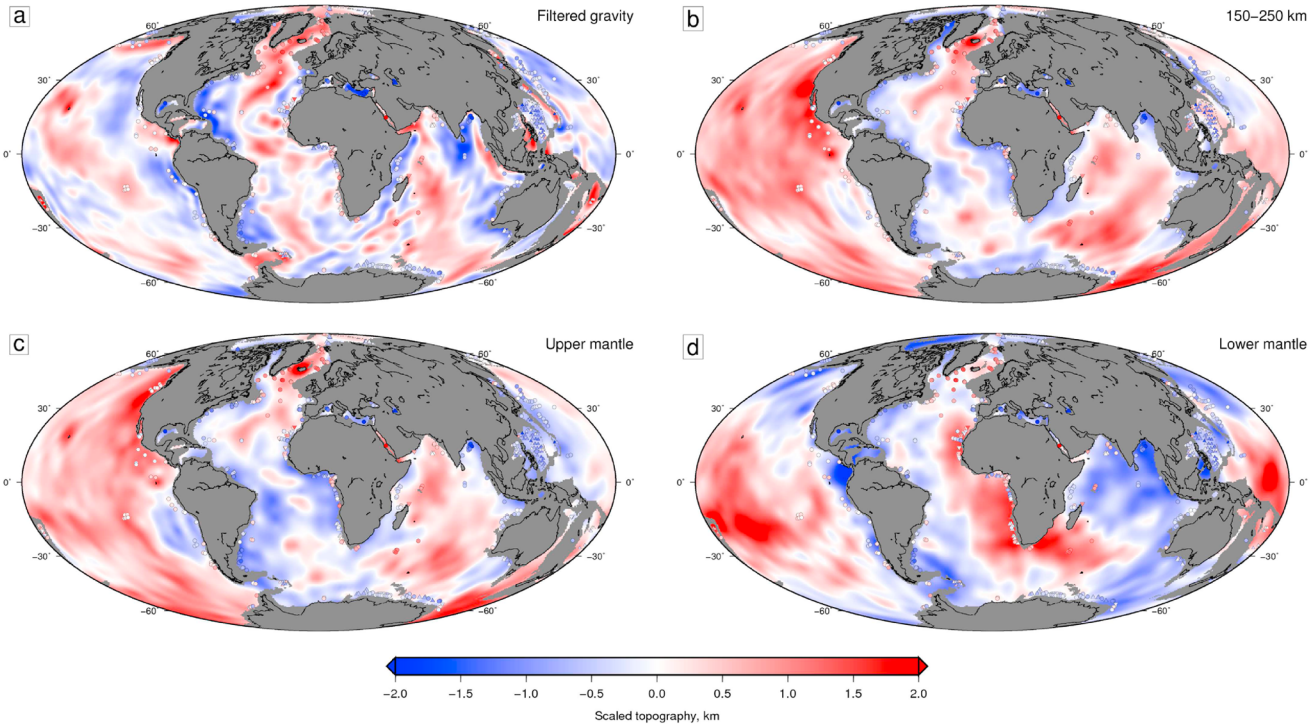

Figure 12. Predicted residual depth using linear relationships from Figures 10a and 10e (Hammer Equal Area projection). (a) Residual depth calculated from long-wavelength gravity anomalies using $\Delta D_g = 0.046\, g + 0.092$. Red colors = negative (i.e., shallow) residual depth; blue colors = positive (i.e., deep) residual depth. Filled circles and triangles = locations of accurate measurements of residual depth. $r = 0.6$. (b) Predicted residual depth from S40RTS shear velocity anomalies averaged between 150 and 250 km using $\Delta D_v = -0.66\overline{\Delta V_s} - 0.23$. $r = 0.4$. (c) Predicted residual depth variation for upper mantle using $\Delta D_v = -0.96\overline{\Delta V_s} - 0.12$. $r = 0.1$. (d) Predicted residual depth variation for lower mantle using $\Delta D_v = -2.79\overline{\Delta V_s} - 0.22$. $r = 0.4$.

$V_s^{obs}(Z)$ and $V_s^{ref}(Z)$ are the observed and reference shear velocities at a depth Z km, respectively. For a depth range of $Z_{min} - Z_{max}$ km sampled at intervals of Z_{int} km, Z is given by

$$Z = Z_{min} + Z_{int}(i - 1) \tag{10}$$

and N by

$$N = \frac{Z_{max} - Z_{min}}{Z_{int}} + 1. \tag{11}$$

The correlation coefficients are −0.5 and −0.4 for the whole mantle and the upper mantle, respectively. There is almost no correlation between velocities, averaged over any portion of the mantle, and gravity anomalies (Figure 10f).

In Figure 11, the relationship between residual depth measurements and the sign of gravity and average velocity anomalies is shown as a function of plate age. For long-wavelength gravity anomalies, ~80% of spot measurements have the correct sign, which suggests that these anomalies are a reasonable proxy for the distribution of residual topography within the oceanic realm. For average velocity anomalies integrated over the upper, lower, and whole mantle, ~60% of the spot measurements have the correct sign.

We examined the empirical correlation between residual depth measurements and several other global and regional tomographic models [e.g., *Grand*, 2002; *Li et al.*, 2008; *Fishwick*, 2010]. *Grand*'s [2002] TXBW model, which incorporates *S* wave and higher-order *S* wave arrivals, has a whole mantle correlation of −0.50. The *Li et al.* [2008] model, which only uses *P* wave arrivals, has a correlation coefficient of −0.1. Finally, we examined the correlation between the regional surface wave tomographic model of *Fishwick* [2010], which encompasses Africa. If shear velocities are averaged for a layer between 125 and 225 km depth, the correlation coefficient is −0.4 and for a horizontal slice at 175 km this value increases to −0.5. The equivalent correlation coefficients for the S40RTS model at these depths are −0.2 and −0.5, respectively. We conclude that the highest correlation coefficients are obtained for the S40RTS tomographic model.

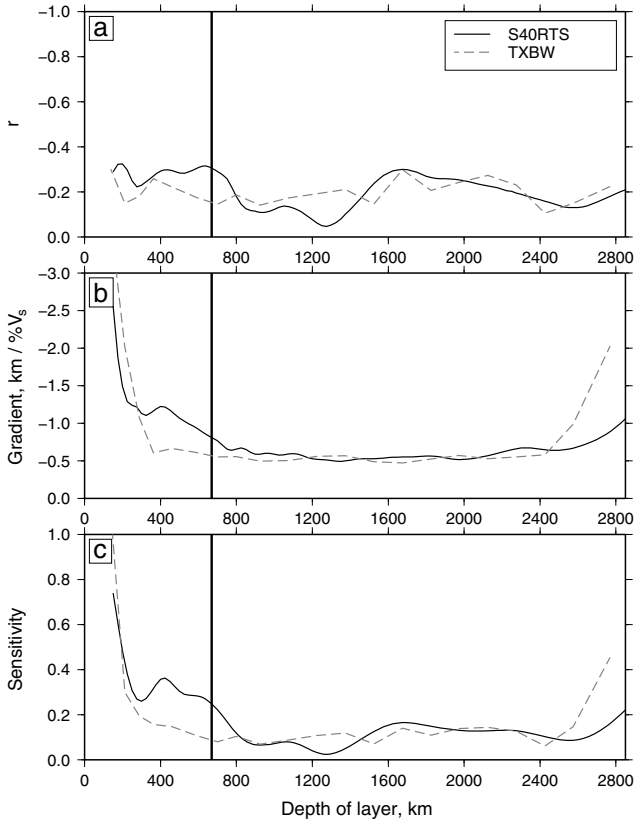

Figure 13. (a) Correlation coefficient between residual depth measurements and velocity anomalies as function of depth. Solid line = S40RTS; dashed line = TXBW. (b) Gradient of best fitting line, which fits residual depth measurements and velocity anomalies as function of depth. (c) Product of correlation coefficient and best fitting gradient as function of depth.

In Figure 12, the spatial variation of these proxies, which are scaled against our measurements of residual depth using the relationships in Figure 10, are presented. For the long-wavelength gravity field, we assumed $\Delta D_g = 0.05\Delta g + 0.1$ to construct a global variation of residual depth (Figure 12a). As expected, spot measurements of residual depth are broadly in agreement. The best match is along the West African and South American margins. Large discrepancies occur at the Australian-Antarctic Discordance and along the west coast of India. Elsewhere, the calibrated gravity field appears to be a reasonable proxy for residual depth. A similar style of calibration was applied to velocity anomalies averaged over different depth ranges from the S40RTS model (Figures 12b–12d). Figure 13 summarizes the way in which residual depth measurements and velocity anomalies correlate as a function of depth. These empirical predictions adequately match spot measurements of residual depth. However, there are important differences. Notably, short-wavelength variations of residual depth along the West African coastline are matched by gravity anomalies, but they are not resolved by the S40RTS model. Such discrepancies emphasize the difficulties faced when constructing geodynamical predictions from tomographic models.

6. Discussion

The global pattern of residual depth presented here differs in significant ways from previously published work [e.g., *Mùller et al.*, 2008; *Crosby and McKenzie*, 2009; *Flament et al.*, 2013]. It is useful to compare our distribution with Figure 1 of *Flament et al.* [2013] which summarizes four different residual topographic fields. The main differences are primarily along continental margins since our database of seismic reflection and wide-angle profiles is concentrated along the oldest oceanic floor. For example, around the African coastline, we have accurately resolved the amplitude and wavelength of residual depth. Since these residual depth anomalies intersect the coastline, they provide important constraints for the onshore distribution of residual topography which is harder to measure [*Al-Hajri et al.*, 2009]. Along the eastern margin of the North and South America, the extent of negative residual topography is much greater than previously thought. Many other small but significant differences occur.

Our intention is to build a database of accurate residual depth measurements. Consequently, gaps and omissions are important features of the global maps presented here. We have carefully and deliberately excised regions where residual depth is either uncertain or unknown. Most of these regions comprise either thickened oceanic crust where wide-angle constraints are not available, or thickly sedimented margins where deep seismic reflection profiles are not yet available. In future, we hope to be able to seed these regions with measurements.

Our results have important implications. Considerable effort has been put into building sophisticated geodynamical models, which predict dynamic topography from the density distribution within the convecting mantle [e.g., *Flament et al.*, 2013]. Convenient starting points for density distribution are either slab-based descriptions based upon a history of subduction or density anomalies calculated from seismic tomographic models. Predicted dynamic topography is strongly dependent upon the assumed viscosity of the mantle. The global pattern of residual topography is a useful test of published models which differ from each other in important ways. A set of typical models are shown in Figure 4 of *Flament et al.* [2013]. Three of these models predict that present-day dynamic topography varies with an amplitude of about ±2000 m [*Flament et al.*, 2013; *Steinberger*, 2007; *Spasojevic and Gurnis*, 2012]. In contrast, *Ricard et al.* [1993] and *Conrad and Husson* [2009] have ranges of −1600 to +600 m and −1550 to +1450 m. All five models share a number of important features. First, they are dominated by a series of very long wavelength swells and depressions, notably the Southern Ocean and Pacific Ocean superswells, which are separated by drawn-down regions centered on Southeast Asia and South America.

The most significant discrepancy between observed and predicted dynamic topography occurs in Southeast Asia. Here a region of ∼2 km of dynamic drawdown, which stretches from the Northeast Shelf of Australia to the South China Sea, and from the east coast of India to the Marianas Trench, is a feature of most predictive models. Although this region is dominated by negative residual depth anomalies, the average amplitude is about −500 m and important short-wavelength variation exists. In the center of this region, there is geologic evidence that Borneo has been rapidly uplifted in Neogene times (C. Meehan, written communication, 2012).

In the North Atlantic Ocean, *Conrad et al.* [2004] used the S20RTS and TXBW tomographic models to predict dynamic topography generated by the Icelandic and Azorean plumes. Once again, there are important discrepancies between predicted and observed dynamic topography. For example, Figure 5 shows that residual depth is asymmetrically distributed on either side of the Reykjanes Ridge south of Iceland with greater positive residual topography on the European plate. Predictive models usually have the opposite sense of asymmetry. Further south, the position of the Azorean plume is incorrect, and the Newfoundland margin is predicted to be drawn down with respect to the Iberian margin by 400–600 m. The observed sense of drawdown is the other way around with an amplitude of 1 km. We concur that some of these differences may reflect differences in spherical harmonic degree.

A detailed analysis of a region encompassing the African plate was carried out by *Gurnis et al.* [2000] who used the S20RTS tomographic model as a starting point. Their model predicts the long-wavelength growth of dynamic topography for subequatorial Africa, but short wavelength variations along the coastline are not resolved. *Conrad and Gurnis* [2003] revisited this problem and determined a history of dynamic topography from 75 Ma to the present day. However, this revised model does not agree with spot measurements of residual depth [*Al-Hajri et al.*, 2009]. *Daradich et al.* [2003] focus on northeast Africa and the Arabian peninsula using both the S20RTS and TXBW tomographic models. Their predictions broadly agree with their observed residual topography, which is slightly smaller than our spot measurement from the Red Sea. Finally, *Forte et al.* [2010] predict dynamic topography for the whole of Africa using two different seismic tomographic models and a range of radial viscosity functions. In all four cases, there are significant discrepancies between prediction and observation, especially at the coastline.

7. Conclusions

We have built a database of seismic reflection and wide-angle profiles in order to constrain residual depth at well-sedimented margins throughout the oceanic realm. Accurate estimates of residual depth depend upon our ability to strip out the isostatic effects of sedimentary loads as well as crustal and lithospheric thickness variations. Our analysis has yielded 449 measurements of residual topography, which are evenly distributed from 0 to > 200 Ma oceanic plates. Many of our measurements are adjacent to continents, which helps to constrain the variation of onshore residual topography.

We have used these measurements in conjunction with selected ship track bathymetric data to construct a global map of residual topography in the oceanic realm. The relationships between residual depth, long-wavelength gravity anomalies, and seismic tomographic models, such as S40RTS, have been explored. Our results are partly encouraging, but they also highlight the limitations of using seismic tomographic models as the exclusive basis of dynamic topographic predictions. Although there is some

correlation between averaged seismic velocity anomalies and residual depth, it is weak, and there are many shorter-wavelength features (~1800 km) which have not yet been tomographically resolved.

Our residual topographic maps show that there are significant discrepancies with published predictions of present-day dynamic topography and observations of residual depth anomalies. Most of these predictive models are concerned with matching dynamic topographic measurements on the continents, and they often neglect oceanic constraints. We emphasize the importance of obtaining accurate spatial and temporal measurements of residual depth, of exploring the phenomenological links between different data sets, and of the need to improve geodynamical models. It is vital that future modeling endeavors pay greater attention to the matching of observations.

Appendix A: Global Database

Tables A1 and A3 summarize data sources used to determine spot measurements of residual topography (Figure 5). When individual profiles span more than one 2° × 2° cell, multiple values of residual depth are given. Data may differ from points on map where individual cells are constrained by multiple profiles. For each profile, digitized seabed, sediment-basement interface, and base of oceanic crust is shown in Figure A1. Point data (i.e., where sediment and crustal thickness are known from spot measurements) are shown in Table A2, and points corrected for flexure are shown in Table A3.

Table A1. Profiles Recorded in Depth

Profile	Reference	Longitude	Latitude	Z_w, m	Z_s, m	Z_c, m	Age, Ma	Z_{wl}, m	Z_{res}, m
228	*Jokat et al.* [2004]	6.00	−67.01	4304	835	10690	139	5510	146
228	*Jokat et al.* [2004]	6.00	−67.64	4307	873	8818	143	5191	479
229	Proprietary data	302.21	−46.83	3707	5522	5354	131	6237	−646
229	Proprietary data	302.76	−46.71	4052	4570	5140	130	6147	−569
230	Proprietary data	305.50	−41.31	4759	2932	6831	126	6410	−871
231	Proprietary data	306.72	−39.59	4755	2968	5928	125	6257	−727
232	Proprietary data	302.30	−46.56	3634	5809	5807	131	6363	−774
232	Proprietary data	302.73	−47.25	4058	4539	5082	130	6129	−551
232	Proprietary data	302.90	−47.52	4202	4085	3974	129	5868	−295
233	Proprietary data	305.24	−40.96	4676	2895	8402	130	6598	−1014
234	*Ehlers and Jokat* [2009]	16.25	85.34	3660	187	no data	3	3786	−563
234	*Ehlers and Jokat* [2009]	20.00	84.26	4047	708	no data	27	4511	−125
234	*Ehlers and Jokat* [2009]	24.30	83.01	4034	2062	no data	47	5285	−382
234	*Ehlers and Jokat* [2009]	26.75	82.31	3863	3219	no data	51	5704	−717
234	*Ehlers and Jokat* [2009]	27.99	81.95	3537	2993	no data	56	5268	−171
235	*Ehlers and Jokat* [2009]	100.50	87.59	4421	1247	no data	46	5213	−320
235	*Ehlers and Jokat* [2009]	105.00	87.80	4415	1749	no data	50	5495	−536
235	*Ehlers and Jokat* [2009]	110.00	88.03	4407	1488	no data	52	5340	−324
235	*Ehlers and Jokat* [2009]	115.00	88.26	4387	2071	no data	54	5644	−587
235	*Ehlers and Jokat* [2009]	120.00	88.49	4365	1594	no data	55	5358	−277
235	*Ehlers and Jokat* [2009]	125.00	88.72	4343	1593	no data	55	5335	−256
235	*Ehlers and Jokat* [2009]	129.20	88.92	4325	868	no data	57	4889	218
235	*Ehlers and Jokat* [2009]	75.05	86.42	3922	13	no data	5	3930	−549
235	*Ehlers and Jokat* [2009]	80.00	86.65	3260	21	no data	15	3274	652
235	*Ehlers and Jokat* [2009]	85.00	86.88	3678	21	no data	22	3693	520
235	*Ehlers and Jokat* [2009]	90.00	87.11	4323	615	no data	32	4729	−195
235	*Ehlers and Jokat* [2009]	95.00	87.34	4428	865	no data	39	4990	−266
235	*Ehlers and Jokat* [2009]	97.95	87.47	4424	1564	no data	44	5400	−563
236	*Ehlers and Jokat* [2009]	27.35	83.73	4054	1394	no data	42	4932	−125
236	*Ehlers and Jokat* [2009]	28.70	83.08	3988	2770	no data	49	5608	−650
236	*Ehlers and Jokat* [2009]	31.00	81.98	3436	3679	no data	57	5494	−377
237	*Ehlers and Jokat* [2009]	1.25	79.55	2705	703	no data	7	3166	374
237	*Ehlers and Jokat* [2009]	3.75	79.32	2788	303	no data	1	2992	−28
237	*Ehlers and Jokat* [2009]	356.65	79.98	2597	2156	no data	22	3899	327
237	*Ehlers and Jokat* [2009]	358.70	79.79	2783	1856	no data	16	3923	88
238	*Ehlers and Jokat* [2009]	357.30	77.76	3025	2618	no data	32	4568	−27
238	*Ehlers and Jokat* [2009]	358.10	77.61	3096	2478	no data	32	4568	−10
238	*Ehlers and Jokat* [2009]	1.25	77.05	3236	1244	no data	24	4026	264

Table A1. (continued)

Profile	Reference	Longitude	Latitude	Z_w, m	Z_s, m	Z_c, m	Age, Ma	Z_{wl}, m	Z_{res}, m
238	*Ehlers and Jokat* [2009]	4.50	76.46	2809	358	no data	12	3049	771
238	*Ehlers and Jokat* [2009]	359.35	77.39	3160	1231	no data	31	3943	577
239	*Ritzmann et al.* [2004]	5.50	78.70	1809	3257	3563	6	3016	406
239	*Ritzmann et al.* [2004]	7.58	78.77	1157	5616	3058	21	3302	886
240	*Barton and White* [1997]	335.54	56.87	3034	1227	9016	49	4168	772
241	*Bauer et al.* [2000]	11.63	−24.11	3319	2922	9880	123	5527	−25
242	*Bauer et al.* [2000]	11.54	−24.93	3803	2861	7915	121	5619	−140
243	*Breivik et al.* [2006]	356.84	65.99	3445	975	3942	33	3493	1087
243	*Breivik et al.* [2006]	358.62	65.41	3086	1585	5100	48	3705	1220
244	*Canales et al.* [2003]	255.84	8.70	3053	0	6201	0	2887	−220
245	*Canales et al.* [2003]	255.71	9.29	3040	0	6464	0	2923	−310
246	*Canales et al.* [2003]	255.94	9.21	2982	0	6701	0	2908	−152
247	*Canales et al.* [2003]	255.59	9.26	2890	0	7038	0	2878	−204
248	*Canales et al.* [1998]	246.34	−15.90	3114	0	5736	1	2862	77
248	*Canales et al.* [1998]	248.01	−15.66	3233	0	5881	4	3008	286
249	*Canales et al.* [1998]	245.72	−17.42	3100	0	5210	2	2751	274
249	*Canales et al.* [1998]	244.77	−17.54	3165	0	5301	3	2834	346
250	*Canales et al.* [1998]	247.22	−17.23	3093	0	5479	0	2794	−27
250	*Canales et al.* [1998]	247.68	−17.17	3150	0	5422	1	2840	113
251	*Collier et al.* [2009]	56.95	−2.14	4523	267	5358	59	4382	788
251	*Collier et al.* [2009]	56.45	−2.90	4273	554	5378	61	4323	880
252	*Collier et al.* [1998]	339.08	27.88	4718	1775	7444	135	5875	−248
253	*Collier et al.* [1998]	339.10	27.97	4664	1468	7822	135	5718	−90
254	*Collier et al.* [1998]	339.18	28.04	4724	1362	7392	136	5638	−7
255	*Collier et al.* [1998]	339.19	27.89	4714	1788	6625	136	5728	−95
256	*Collier et al.* [1998]	339.20	27.98	4678	1669	6853	136	5668	−35
257	*Contreras-Reyes et al.* [2008]	283.08	−37.47	4100	291	7159	29	4307	155
257	*Contreras-Reyes et al.* [2008]	284.02	−37.67	4102	360	7449	30	4408	79
258	*Contrucci et al.* [2004]	349.54	34.45	4194	3954	8892	177	6708	−985
259	*Cooper et al.* [1992]	177.20	58.76	3640	4309	6557	77	5881	−331
259	*Cooper et al.* [1992]	177.20	56.88	3913	3023	8490	73	5914	−432
260	*Cooper et al.* [1992]	182.04	54.96	3803	4575	no data	68	6261	−891
260	*Cooper et al.* [1992]	183.76	55.86	3801	4125	no data	69	6061	−658
261	*Corredor et al.* [2005]	5.63	3.17	2397	7250	no data	99	5912	−437
262	*Crosby et al.* [2010]	227.59	71.62	1189	14302	no data	140	7007	−1348
263	*Ebeniro et al.* [1988]	266.00	25.97	3063	12569	4880	169	7941	−2226
264	*Edwards et al.* [1997]	359.76	4.29	4933	2950	4135	94	6096	−556
265	*Gerlings et al.* [2011]	318.32	48.47	4320	1633	4990	86	4946	666
266	*Gailler et al.* [2009]	5.72	41.11	2642	6680	5452	16	5642	−1634
267	*Gailler et al.* [2009]	6.39	39.86	2729	5567	3419	22	4921	−678
269	*Greenroyd et al.* [2007]	309.70	7.56	4193	4049	4091	89	5865	−272
269	*Greenroyd et al.* [2007]	309.13	6.77	3537	5642	4043	95	5875	−350
270	*Hampel et al.* [2004]	283.20	−15.70	3131	210	15159	45	4758	103
271	*Hampel et al.* [2004]	283.23	−15.64	2980	314	16270	45	4882	−19
272	*Hirata et al.* [1992]	138.21	42.61	3684	1930	6388	17	4732	−684
272	*Hirata et al.* [1992]	136.88	42.04	3739	2002	6799	18	4903	−819
272	*Hirata et al.* [1992]	137.72	42.40	3746	1949	6515	17	4829	−782
273	*Hirsch et al.* [2009]	14.38	−32.99	3374	2622	7008	126	4902	633
274	*Holbrook and Kelemen* [1993]	286.28	36.28	2758	10108	4608	177	6801	−1079
275	*Holbrook and Kelemen* [1993]	288.36	38.15	2512	9251	8215	174	6935	−1216
276	*Holbrook and Kelemen* [1993]	284.09	32.45	3976	4890	7413	180	6626	−902
277	*Holbrook and Kelemen* [1993]	188.25	50.35	5510	1703	4739	63	6129	−872
278	*Hopper et al.* [2003]	316.86	46.08	4526	1494	3755	108	4845	554
279	*Klingelhöfer et al.* [2000]	4.50	71.44	3023	939	4310	21	3116	1063
280	*Klingelhöfer et al.* [2000]	4.09	71.64	3019	521	4465	17	2880	1141

Table A1. (continued)

Profile	Reference	Longitude	Latitude	Z_w, m	Z_s, m	Z_c, m	Age, Ma	Z_{wl}, m	Z_{res}, m
282	*Klingelhöfer et al.* [2008]	339.95	23.49	3838	4113	7702	158	6205	−503
283	*Klingelhöfer et al.* [2008]	341.46	22.93	3097	6680	7390	170	6454	−738
284	*Kopp et al.* [2002]	106.07	−9.67	5715	644	7317	104	6180	−758
285	*Korenaga et al.* [2000]	328.48	64.61	2255	929	10498	43	3483	1337
287	*Lau et al.* [2006]	313.66	44.40	3993	2765	4365	124	5106	407
288	*Lizarralde and Holbrook* [2002]	196.34	52.66	5887	1063	6004	56	6368	−1269
288	*Lizarralde and Holbrook* [2002]	196.50	52.42	5126	1185	5763	56	5635	−540
289	*Lizarralde et al.* [2007]	251.80	23.29	2599	1888	4904	3	3351	−169
290	*Lizarralde et al.* [2007]	251.10	22.61	2917	1357	4904	3	3368	−150
290	*Lizarralde et al.* [2007]	251.91	22.18	2923	1476	4295	6	3331	111
290	*Lizarralde et al.* [2007]	252.62	21.79	2800	1912	4464	8	3484	116
291	*Lizzaralde and Holbrook* [1997]	286.10	36.48	2483	7522	8572	179	6368	−644
292	*Lizzaralde and Holbrook* [1997]	286.30	36.44	3017	6965	7551	178	6510	−787
293	*Navin et al.* [1998]	327.17	57.78	1602	13	7491	1	1684	1280
293	*Navin et al.* [1998]	327.83	57.60	1557	96	6968	4	1599	1674
293	*Navin et al.* [1998]	328.24	57.48	2061	11	6362	7	1932	1577
294	*Páramo et al.* [2008]	251.19	22.62	2953	1245	7924	3	3896	−671
294	*Páramo et al.* [2008]	251.63	22.40	2734	1282	8077	5	3727	−359
295	*Parsiegla et al.* [2009]	25.34	−35.88	4291	561	8035	115	4835	588
296	*Parsiegla et al.* [2009]	24.04	−36.72	4692	133	7200	116	4801	623
297	*Parsiegla et al.* [2009]	288.38	−20.99	5442	752	4744	52	5500	−480
299	Proprietary data	318.48	−31.35	3858	2387	6150	105	5107	306
300	Proprietary data	310.52	−32.48	773	10812	7348	132	5551	54
300	Proprietary data	310.43	−32.57	597	11071	7671	133	5517	92
301	*Chian and Louden* [1994]	308.62	59.94	3300	1876	6708	64	4378	900
303	*Rodger et al.* [2006]	312.35	4.45	2524	8916	4244	97	6101	−599
303	*Rodger et al.* [2006]	313.38	5.39	3467	4588	6426	81	5806	−205
306	*Scherwath et al.* [2009]	282.04	−43.12	3563	84	5432	8	3313	293
306	*Scherwath et al.* [2009]	283.13	−42.99	3579	237	5578	10	3459	263
307	*Scherwath et al.* [2009]	282.20	−44.89	2809	153	4674	1	2466	374
307	*Scherwath et al.* [2009]	283.12	−44.71	2983	282	5527	3	2883	268
308	*Scherwath et al.* [2009]	283.10	−45.86	2277	182	4305	1	1886	893
309	*Funck et al.* [2003]	316.75	46.11	4387	1744	2361	109	4590	808
310	*Shillington et al.* [2006]	315.88	45.06	4697	1326	3230	111	4822	577
311	*Shillington et al.* [2006]	316.04	45.08	4747	1481	no data	110	5676	−277
312	*Shillington et al.* [2006]	315.82	44.96	4708	1427	no data	111	5606	−206
313	*Hopper et al.* [2003]	323.02	62.51	1995	1515	12752	50	3985	991
313	*Hopper et al.* [2003]	323.63	62.31	2332	1382	10828	49	3890	1054
314	*Holbrook et al.* [2001]	318.93	58.69	2856	1140	9444	49	4017	932
315	*Funck et al.* [2004]	302.32	41.98	4709	4535	3914	163	6562	−855
315	*Funck et al.* [2004]	302.58	41.43	4931	3780	4189	158	6499	−797
316	*Wu et al.* [2006]	299.83	41.38	4574	4780	4669	168	6672	−958
317	*Louden and Chian* [1999]	305.69	56.87	2963	3046	4943	60	4322	856
318	*Tsikalas et al.* [2005]	7.09	69.31	3098	1386	6940	49	3942	1006
319	*Tsikalas et al.* [2005]	7.28	70.22	2998	2046	5426	41	3932	842
319	*Tsikalas et al.* [2005]	7.85	70.00	3007	1951	5519	42	3907	890
320	*Tsikalas et al.* [2005]	11.11	69.63	2848	2576	7775	51	4493	486
321	*Tsuru et al.* [2000]	145.37	38.96	5302	324	6007	132	5319	284
322	*Turner et al.* [1999]	183.22	−22.41	2415	0	8057	0	2592	158
323	*Turner et al.* [1999]	183.39	−22.20	2171	0	8801	0	2484	158
324	*Moulin et al.* [2005]	9.74	−6.83	3565	6078	5410	117	6326	−886
325	*Moulin et al.* [2005]	10.21	−8.04	3980	3423	5810	119	5680	−226
326	*Moulin et al.* [2005]	10.18	−7.43	3896	4369	5736	119	6013	−557
326	*Moulin et al.* [2005]	9.47	−7.58	4117	3542	6974	116	6088	−663
327	*Zelt et al.* [2003]	286.77	−32.79	4150	869	5793	38	4474	220

Table A2. Results From 1-D Refraction Profiles and Similar

Reference	Longitude	Latitude	Z_w, ms	Z_s, ms	Z_c, ms	Age, Ma	Z_{wl}, m	Z_{res}, m
DeVoogd et al. [1992]	17.49	36.14	3,470	6,819	9,180	245.2	7,209	−1464
DeVoogd et al. [1992]	18.03	35.66	3,816	5,066	8,289	241.2	6,701	−955
DeVoogd et al. [1992]	28.19	33.21	2,966	10,000	10,677	266	8,092	−2351
Minshull and White [1996]	61.50	−31.54	4,100	0	4,300	32.5	3,584	977
Minshull and White [1996]	62.60	−31.35	4,160	0	5,400	35.7	3,847	799
Chamot-Rooke et al. [1993]	81.28	−2.64	4,827	1,683	5,534	80	5,628	−40
Chamot-Rooke et al. [1993]	81.34	−1.95	4,807	2,436	5,584	81	6,003	−414
Chamot-Rooke et al. [1993]	81.34	−1.48	4,775	2,648	6,391	83	6,292	−694
Chamot-Rooke et al. [1993]	81.34	−1.06	4,727	2,751	6,602	84	6,330	−718
Chamot-Rooke et al. [1993]	81.34	−0.58	4,626	2,603	7,108	87	6,196	−588
Cambridge holdings	155.16	36.81	5,724	735	7,059	135.8	6,198	−565
Cambridge holdings	56.28	36.34	5,539	372	5,919	137.5	5,571	73
Cambridge holdings	54.68	34.02	5,786	620	4,402	146.3	5,698	−17
Cambridge holdings	53.65	33.98	5,916	583	5,487	142.5	6,004	−335
Cambridge holdings	52.20	33.90	5,919	292	5,928	144.8	5,900	−223
Cambridge holdings	51.36	34.03	5,955	627	4,379	144.2	5,867	−192
Cambridge holdings	50.58	34.03	5,972	666	4,857	143.5	5,997	−324
Cambridge holdings	48.88	33.96	6,161	614	4,991	142.8	6,177	−507
Cambridge holdings	51.62	33.94	5,947	841	4,219	144.5	5,963	−287
Cambridge holdings	50.95	34.10	5,951	576	4,863	143.7	5,920	−247
Cambridge holdings	50.43	34.08	5,971	260	4,793	143.3	5,721	−49
Cambridge holdings	49.38	33.98	6,167	801	3,493	143.0	6,025	−354
Cambridge holdings	48.74	34.05	6,154	547	4,541	142.6	6,045	−376
Cambridge holdings	52.25	33.85	5,970	645	4,062	144.9	5,835	−158
Cambridge holdings	64.42	32.69	6,195	468	3,499	137.3	5,843	−200
Cambridge holdings	63.89	32.07	6,041	566	3,045	139.6	5,668	−12
Cambridge holdings	47.32	30.68	6,135	314	5,588	146.8	6,067	−384
Cambridge holdings	49.06	37.60	5,812	764	4,808	136.5	5,889	−251
Cambridge holdings	49.40	37.46	5,880	1,027	4,855	136.8	6,127	−487
Cambridge holdings	50.24	36.95	5,670	552	6,236	137.6	5,876	−231
Cambridge holdings	50.46	36.77	5,663	563	6,234	137.9	5,876	−229
Cambridge holdings	50.13	36.52	5,858	391	5,441	139.0	5,814	−161
Cambridge holdings	51.41	36.63	5,816	406	7,383	136.6	6,140	−502

Table A3. Points Corrected for Flexure Using Results of *Bry and White* [2007]

Reference	Longitude	Latitude	Z_w, m	Z_s, m	Z_c, m	Age, Ma	C_{flex}, m	Z_{wl}, m	Z_{res}, m
Pavlenkova et al. [2009]	288.38	−20.99	5482	725	4734	52.5	−490	5031	49
Contreras-Reyes et al. [2008]	284.13	−37.69	4045	356	7359	30	173	4505	−17
Hampel et al. [2004]	283.76	−16.14	3468	158	13590	45.1	88	4860	6
Hampel et al. [2004]	283.06	−15.86	2693	557	16554	44.7	193	4999	−143
Scherwath et al. [2009]	282.58	−43.05	3516	138	5728	9.5	125	3482	186
Scherwath et al. [2009]	282.81	−44.77	2918	282	5195	2.0	173	2929	156
Scherwath et al. [2009]	283.11	−45.85	2297	167	4326	0.5	186	2085	688
Zelt et al. [2003]	286.84	−32.79	4146	828	6086	37.7	−153	4344	351
Holbrook et al. [1999]	188.39	50.17	5237	1626	4706	63.9	254	6061	−786
Lizarralde and Holbrook [2002]	196.45	52.49	5291	1129	5799	54.3	−108	5666	−607
Tsuru et al. [2000]	145.41	38.95	5258	404	6046	132.2	384	5718	−115
Kopp et al. [2002]	106.04	−9.73	5691	568	7422	104	11	6137	−716

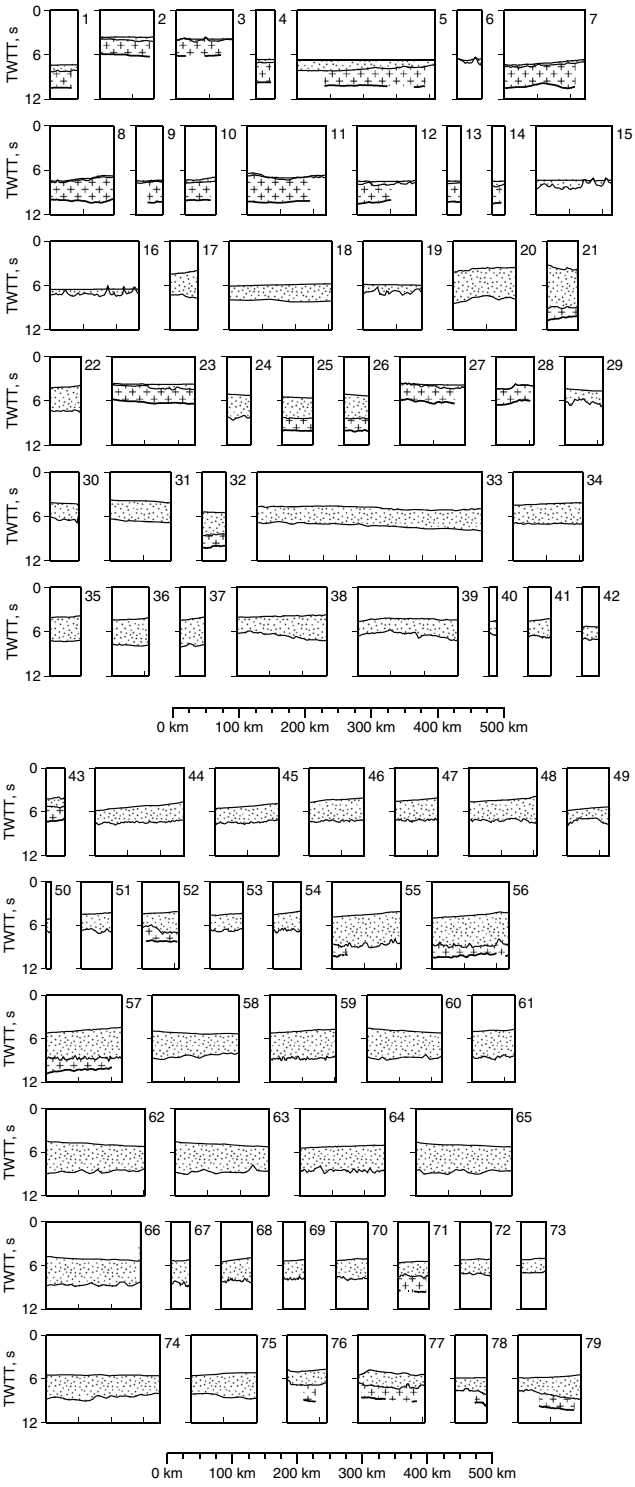

Figure A1. Interpreted seismic images used to create global maps, showing water layer (white), sediment layer (stippled), and igneous crust (crosses). Only oceanic portion of each line is shown. Discontinuous/absent Moho implies that it was unclear or not visible. Profile numbers refer to Tables 1 and A1.

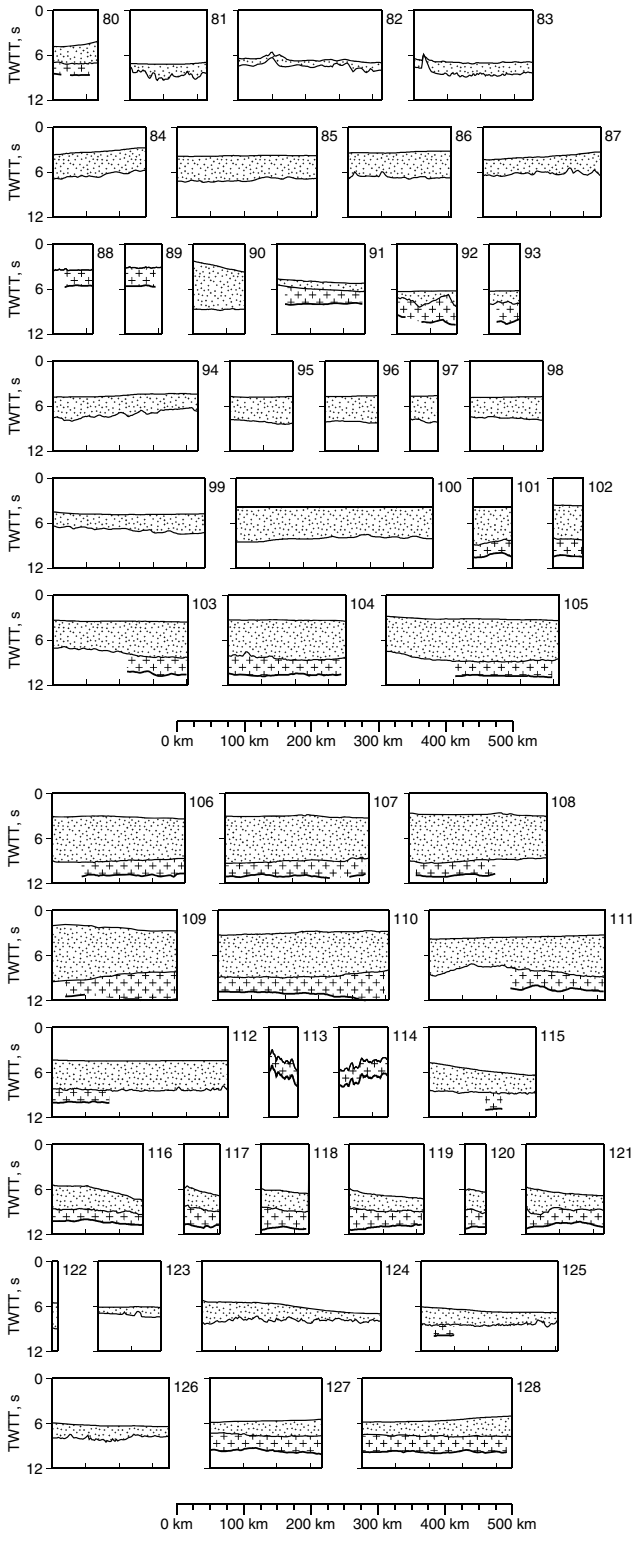

Figure A1. (continued)

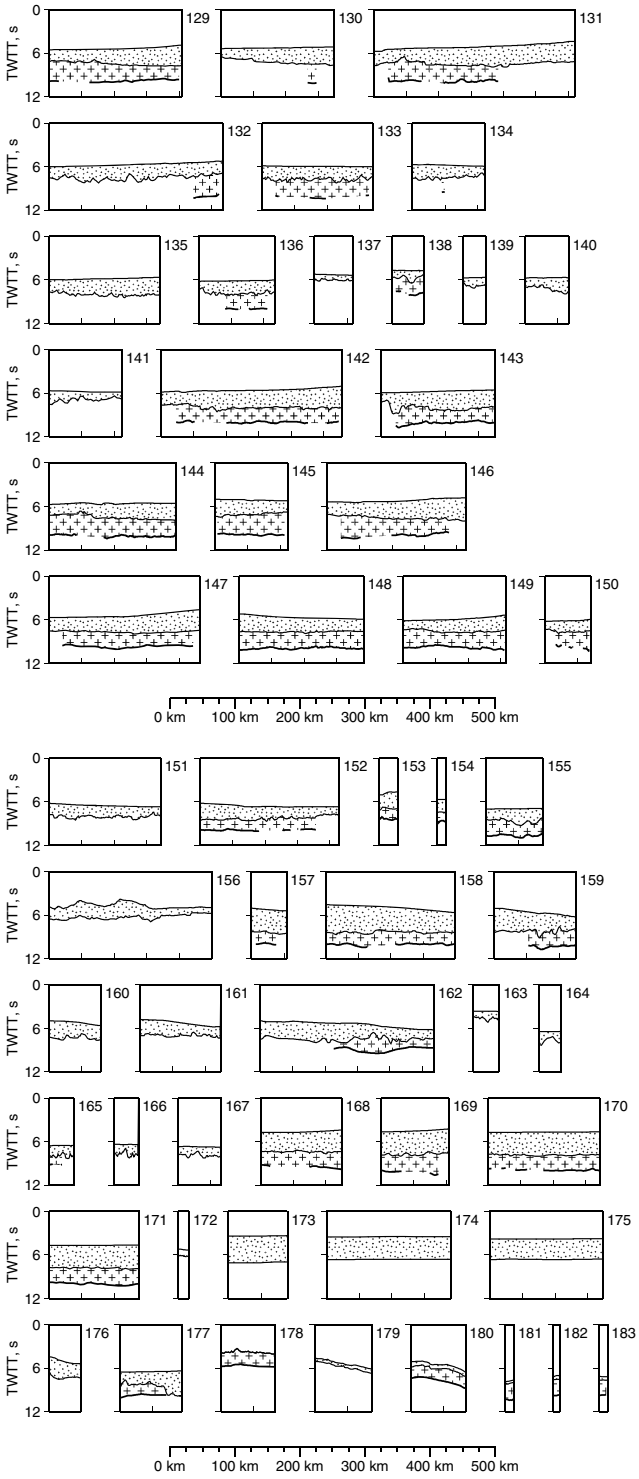

Figure A1. (continued)

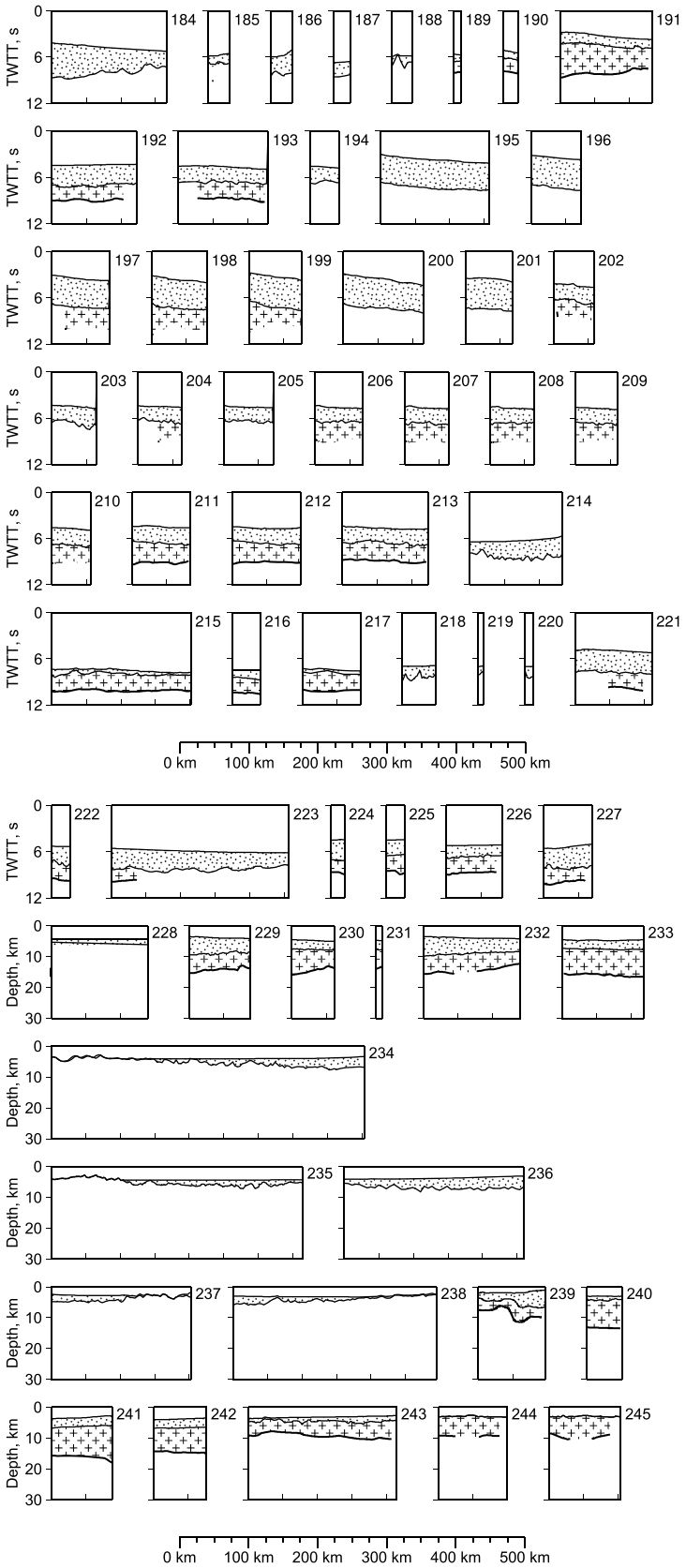

Figure A1. (continued)

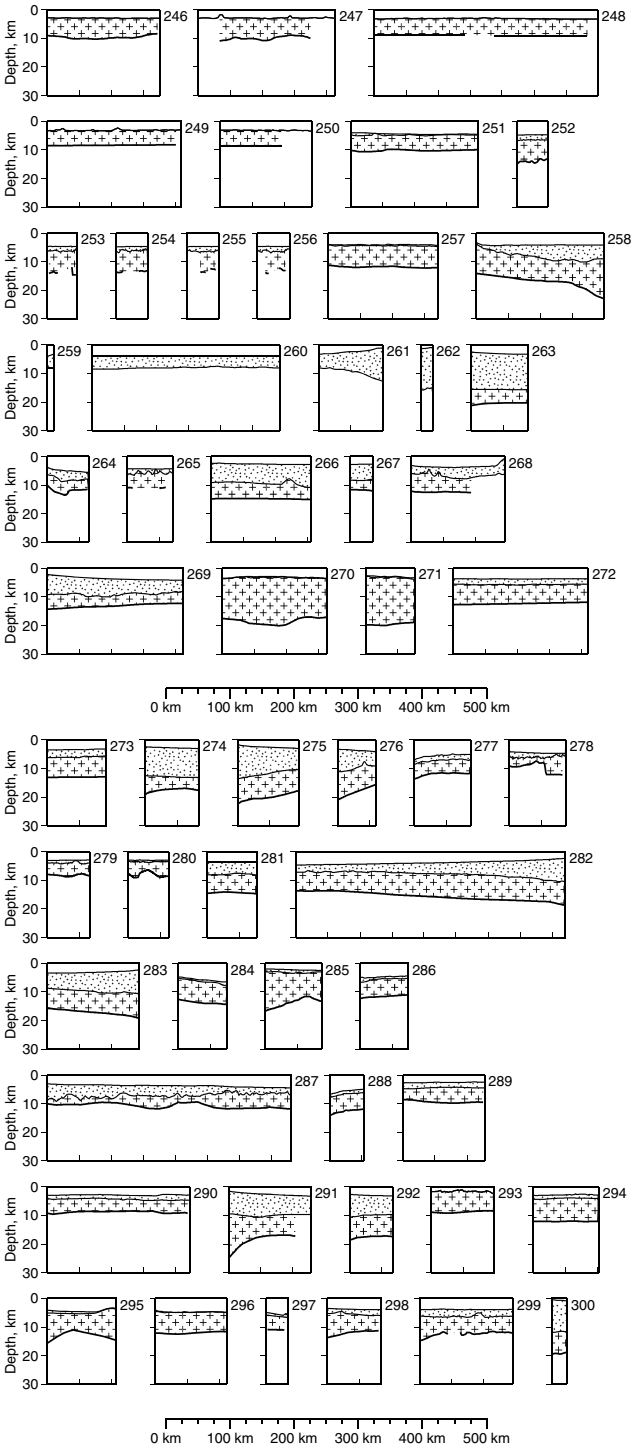

Figure A1. (continued)

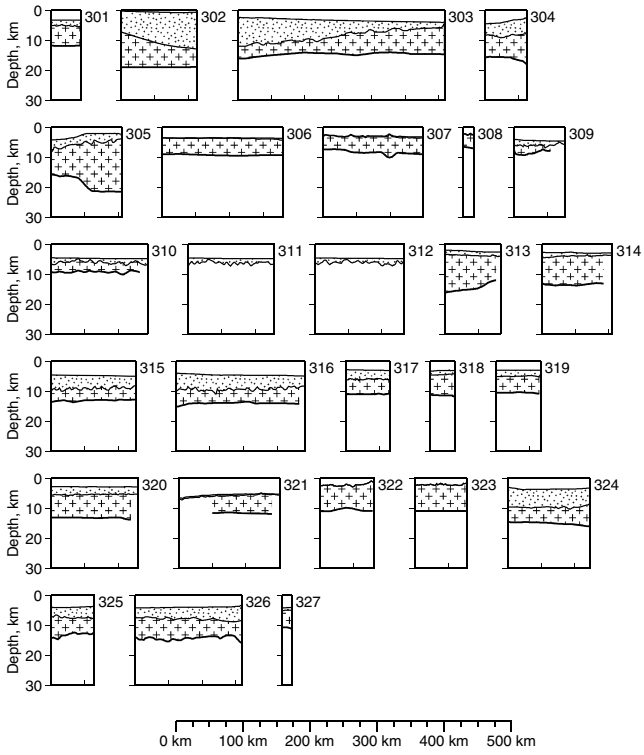

Figure A1. (continued)

Acknowledgments

This work forms part of the BP-Cambridge margins project, which is funded by BP Exploration. We are especially grateful to K. Czarnota and M. Hoggard for constructive discussions. We thank R. Corfield, I. Frame, D. Glassey, C. Lithgow-Bertelloni, D. Lyness, L. Mackay, C. Richardson, G. Roberts, J. Rudge, M. Thompson, and R. White for their help. We are grateful to C. Faccenna, L. Husson, and M. Gurnis for their careful reviews. Cambridge Earth Sciences contribution esc.3026.

References

Al-Hajri, Y., N. White, and S. Fishwick (2009), Scales of transient convective support beneath West Africa, *Geology*, *37*(10), 883–886.

Austin, Jr., J. A., and E. Uchupi (1982), Continental-oceanic crustal transition off southwest Africa, *AAPG Bulletin*, *66*(9), 1328–1347.

Ball, P. J. (2005), Break-up history and evolution of the southern passive margin of Australia, PhD thesis, Royal Holloway University of London.

Barton, A. J., and R. S. White (1997), Crustal structure of Edoras Bank continental margin and mantle thermal anomalies beneath the North Atlantic, *J. Geophys. Res.*, *102*(B2), 3109–3129.

Bassin, C., G. Laske, and G. Masters (2000), The current limits of resolution for surface wave tomography in North America, *EOS Trans. AGU*, *81*, F897.

Bauer, K., S. Neben, B. Schreckenberger, R. Emmermann, K. Hinz, N. Fechner, K. Gohl, A. Schulze, R. B. Trumbull, and K. Weber (2000), Deep structure of the Namibia continental margin as derived from integrated geophysical studies, *J. Geophys. Res.*, *105*, 25,829–25,853.

Becker, T. W., and C. Faccenna (2011), Mantle conveyor beneath the Tethyan collisional belt, *Earth Planet. Sci. Lett.*, *310*(3–4), 453–461. [Available at http://www.sciencedirect.com/science/article/pii/S0012821X11004857.]

Beslier, M., M. Ask, and G. Boillot (1993), Ocean-continent boundary in the Iberia Abyssal Plain from multichannel seismic data, *Tectonophysics*, *218*, 383–393.

Breivik, A. J., R. Mjelde, J. I. Faleide, and Y. Murai (2006), Rates of continental breakup magmatism and seafloor spreading in the Norway Basin-Iceland plume interaction, *J. Geophys. Res.*, *111*, B07102, doi:10.1029/2005JB004004.

Bry, M., and N. White (2007), Reappraising elastic thickness variation at oceanic trenches, *J. Geophys. Res.*, *112*, B08414, doi:10.1029/2005JB004190.

Bunce, E. T., and P. Molnar (1977), Seismic reflection profiling and basement topography in the Somali basin: Possible fracturing zones between Madagascar and Africa, *J. Geophys. Res.*, *82*(33), 5305–5311.

Canales, J. P., R. S. Detrick, S. Bazin, A. J. Harding, and J. A. Orcutt (1998), Off-axis crustal thickness across and along the East Pacific Rise within the MELT area, *Science*, *280*, 1218–1221.

Canales, J. P., G. Ito, R. S. Detrick, and J. Sinton (2002), Crustal thickness along the western Galápagos Spreading Center and the compensation of the Galápagos hotspot swell, *Earth Planet. Sci. Lett.*, *203*, 311–327.

Canales, J. P., R. S. Detrick, D. R. Toomey, and W. S. D. Wilcock (2003), Segment-scale variations in the crustal structure of 150–300 kyr old fast spreading oceanic crust (East Pacific Rise, 8° 15′N–10°5′N) from wide-angle seismic refraction profiles, *Geophys. J. Int.*, *152*, 766–794.

Carbotte, S. M., M. R. Nedimović, J. P. Canales, G. M. Kent, A. J. Harding, and M. Marjanović (2008), Variable crustal structure along the Juan de Fuca Ridge: Influence of on-axis hot spots and absolute plate motions, *Geochem. Geophys. Geosyst.*, *9*(8), Q08001, doi:10.1029/2007GC001922.

Cazenave, A., A. Souriau, and K. Dominh (1989), Global coupling of Earth surface topography with hotspots, geoid and mantle heterogeneities, *Nature*, *340*(6228), 54–57.

Chamot-Rooke, N., F. Jestin, and B. Voogd (1993), Intraplate shortening in the central Indian Ocean determined from a 2100-km-long north-south deep seismic reflection profile, *Geology*, *21*(11), 1043.

Chian, D., and K. E. Louden (1994), The continent-ocean crustal transition across the southwest Greenland margin, *J. Geophys. Res.*, *99*, 9117–9135.

Coffin, M. F., P. D. Rabinowitz, and R. E. Houtz (1986), Crustal structure in the Western Somali basin, *Geophys. J. R. Astron. Soc.*, *86*, 331–369.

Colin, P., and L. Fleitout (1990), Topography of the ocean floor: Thermal evolution of the lithosphere and interaction of deep mantle heterogeneities with the lithosphere, *Geophys. Res. Lett.*, *17*(11), 1961–1964.
Collier, J. S., T. J. Henstock, C. Peirce, and A. B. Watts (1998), A detailed geophysical study in the Canary Basin (eastern Atlantic): Implications for the internal structure of 130 Ma oceanic crust, *Geophys. J. Int.*, *135*, 943–963.
Collier, J. S., and A. B. Watts (2001), Lithospheric response to volcanic loading by the Canary Islands: Constraints from seismic reflection data in their flexural moat, *Geophys. J. Int.*, *147*, 660–676.
Collier, J. S., T. A. Minshull, J. O. S. Hammond, R. B. Whitmarsh, J.-M. Kendall, V. Sansom, C. I. Lane, and G. Rumpker (2009), Factors influencing magmatism during continental breakup: New insights from a wide-angle seismic experiment across the conjugate Seychelles-Indian margins, *J. Geophys. Res.*, *114*, B03101, doi:10.1029/2008JB005898.
Conrad, C. P., and M. Gurnis (2003), Seismic tomography, surface uplift, and the breakup of Gondwanaland: Integrating mantle convection backwards in time, *Geochem. Geophys. Geosyst.*, *4*(3), 1031, doi:10.1029/2001GC000299.
Conrad, C. P., and L. Husson (2009), Influence of dynamic topography on sea level and its rate of change, *Lithosphere*, *1*(2), 110–120.
Conrad, C. P., C. Lithogow-Bertelloni, and K. E. Louden (2004), Iceland, the Farallon slab, and dynamic topography of the North Atlantic, *Geology*, *32*(3), 177–180.
Contreras-Reyes, E., I. Grevemeyer, E. R. Flueh, and C. Reichert (2008), Upper lithospheric structure of the subduction zone offshore of southern Arauco peninsula, Chile, at ~38°S, *J. Geophys. Res.*, *113*, B07303, doi:10.1029/2007JB005569.
Contrucci, I., F. Klingelhöfer, J. Perrot, R. Bartolome, M.-A. Gutscher, M. Sahabi, J. Malod, and J.-P. Rehault (2004), The crustal structure of the NW Moroccan continental margin from wide-angle and reflection seismic data, *Geophys. J. Int.*, *159*, 117–128.
Cooper, A. K., M. S. Marlow, D. W. Scholl, and A. J. Stevenson (1992), Evidence for cenozoic crustal extension in the Bering Sea region, *Tectonophysics*, *11*(4), 719–731.
Corredor, F., J. H. Shaw, and F. Bilotti (2005), Structural styles in the deep-water fold and thrust belts of the Niger Delta, *AAPG Bulletin*, *89*(6), 753–780.
Crosby, A. G., and D. McKenzie (2009), An analysis of young ocean depth, gravity and global residual topography, *Geophys. J. Int.*, *178*, 1198–1219.
Crosby, A. G., D. McKenzie, and J. G. Sclater (2006), The relationship between depth, age and gravity in the oceans, *Geophys. J. Int.*, *166*, 553–573.
Crosby, A. G., S. Fishwick, and N. White (2010), Structure and evolution of the intracratonic Congo Basin, *Geochem. Geophys. Geosyst.*, *11*(6), Q06010, doi:10.1029/2009GC003014.
Cunningham, A. P., R. D. Larter, P. F. Barker, K. Gohl, and F. O. Nitsche (2002), Tectonic evolution of the pacific margin of Antarctica, 2. Structure of Late Cretaceous–early Tertiary plate bound aries in the Bellingshausen Sea from seismic reflection and gravity data, *J. Geophys. Res.*, *107*(B12), doi:10.1029/2002JB001897.
Czarnota, K., M. J. Hoggard, N. White, and J. Winterbourne (2013), Spatial and temporal patterns of cenozoic dynamic topography around Australia, *Geochem. Geophys. Geosyst.*, *14*(3), 634–658, doi:10.1029/2012GC004392.
Daradich, A., J. X. Mitrovica, R. N. Pysklywec, S. D. Willett, and A. M. Forte (2003), Mantle flow, dynamic topography, and rift-flank uplift of Arabia, *Geology*, *31*(10), 901.
Dean, S. M., T. A. Minshull, R. B. Whitmarsh, and K. E. Louden (2000), Deep structure of the ocean-continent transition in the southern Iberia Abyssal Plain from seismic refraction profiles: The IAM-9 transect at 40 degrees 20′N, *J. Geophys. Res.*, *105*(B3), 5859–5885.
DeVoogd, B., C. Truffert, N. Chamotrooke, P. Huchon, S. Lallemant, and X. Lepichon (1992), 2-ship deep seismic-soundings in the basins of the eastern Mediterranean-Sea (PASIPHAE cruise), *Geophys. J. Int.*, *109*, 536–552.
Divins, D. L. (2008), NGDC total sediment thickness of the world's oceans and marginal seas. [Available at http://www.ngdc.noaa.gov/mgg/sedthick/sedthick.html.]
Ebeniro, J. O., Y. Nakamura, D. S. Sawyer, and J. r O'Brien W. P. (1988), Sedimentary and crustal structure of the northwestern Gulf of Mexico, *J. Geophys. Res.*, *93*(B8), 9075–9092.
Edwards, R. A., R. B. Whitmarsh, and R. A. Scrutton (1997), Synthesis of the crustal structure of the transform continental margin of Ghana, northern Gulf of Guinea, *Geo-Mar. Lett.*, *17*, 12–20.
Ehlers, B.-M., and W. Jokat (2009), Subsidence and crustal roughness of ultra-slow spreading ridges in the northern North Atlantic and the Arctic Ocean, *Geophys. J. Int.*, *177*, 451–462.
Fishwick, S. (2010), Surface wave tomography: Imaging of the lithosphere-asthenosphere boundary beneath central and southern Africa?, *Lithos*, *120*(1–2), 63–73.
Flament, N., M. Gurnis, and R. D. Müller (2013), A review of observations and models of dynamic topography, *Lithosphere*, *5*(2), 189–210.
Forte, A. M., S. Quéré, R. Moucha, N. a. Simmons, S. P. Grand, J. X. Mitrovica, and D. B. Rowley (2010), Joint seismic-geodynamic-mineral physical modelling of African geodynamics: A reconciliation of deep-mantle convection with surface geophysical constraints, *Earth Planet. Sci. Lett.*, *295*(3–4), 329–341.
Franke, D., S. Neben, S. Ladage, B. Schreckenberger, and K. Hinz (2007), Margin segmentation and volcanotectonic architecture along the volcanic margin of Argentina/Uruguay, South Atlantic, *Mar. Geol.*, *244*, 46–67.
Funck, T., J. R. Hopper, H. C. Larsen, K. E. Louden, B. E. Tucholke, and W. S. Holbrook (2003), Crustal structure of the ocean-continent transition at Flemish Cap: Seismic refraction results, *J. Geophys. Res.*, *108*(B11), 2531, doi:10.1029/2003JB002434.
Funck, T., H. R. Jackson, K. E. Louden, S. A. Dehler, and Y. Wu (2004), Crustal structure of the northern Nova Scotia rifted continental margin (eastern Canada), *J. Geophys. Res.*, *109*, B09102, doi:10.1029/2004JB003008.
Gailler, A., F. Klingelhöfer, J.-L. Olivet, and D. Aslanian (2009), Crustal structure of a young margin pair: New results across the Liguro-Provencal Basin from wide-angle seismic tomography, *Earth Planet. Sci. Lett.*, *286*, 333–345.
Gardner, J. V. (1970), Submarine Geology of the western Coral Sea, *Geol. Soc. Am. Bull.*, *81*, 2599–2614.
Geoscience Australia (2008), *Acreage Release CD-ROM*.
Gerlings, J., K. E. Louden, and H. R. Jackson (2011), Crustal structure of the Flemish Cap Continental Margin (eastern Canada): An analysis of a seismic refraction profile, *Geophys. J. Int.*, *185*(1), 30–48.
Grand, S. P. (2002), Mantle shear-wave tomography and the fate of subducted slabs, *Philos. Trans. R. Soc. London, Ser. A*, *360*(1800), 2475–2491.
Greenroyd, C. J., C. Peirce, M. Rodger, A. B. Watts, and R. W. Hobbs (2007), Crustal structure of the French Guiana margin, West Equatorial Atlantic, *Geophys. J. Int.*, *169*, 964–987.
Gurnis, M., J. X. Mitrovica, J. Ritsema, and H. J. van Heijst (2000), Constraining mantle density structure using geological evidence of surface uplift rates: The case of the African superplume, *Geochem. Geophys. Geosyst.*, *1*, 1020, doi:10.1029/1999GC000035.
Hager, B. H., and M. a. Richards (1989), Long-wavelength variations in Earth's geoid: Physical models and dynamical implications, *Philos. Trans. R. Soc. London, Ser. A*, *328*(1599), 309–327.
Hager, B., R. Clayton, M. Richards, R. Comer, and A. Dziewonski (1985), Lower mantle heterogeneity, dynamic topography and the geoid, *Nature*, *313*(6003), 541–545.

Hampel, A., N. Kukowski, J. Bialas, C. Huebscher, and R. Heinbockel (2004), Ridge subduction at an erosive margin: The collision zone of the Nazca Ridge in southern Peru, *J. Geophys. Res.*, *109*, B02101, doi:10.1029/2003JB002593.

Hayes, D. E. (1988), Age-depth relationships and depth anomalies in the southeast Indian Ocean and South Atlantic Ocean, *J. Geophys. Res.*, *93*(B4), 2937–2954.

Hirata, N., B. Y. Karp, T. Yamaguchi, T. Kanazawa, K. Suyehiro, J. Kasahara, H. Shiobara, M. Shinohara, and H. Kinoshita (1992), Oceanic crust in the Japan Basin of the Japan Sea by the 1990 Japan-USSR expedition, *Geophys. Res. Lett.*, *19*(20), 2027–2030.

Hirsch, K. K., K. Bauer, and M. Scheck-Wenderoth (2009), Deep structure of the western South African passive margin—Results of a combined approach of seismic, gravity and isostatic investigations, *Tectonophysics*, *470*, 57–70.

Hohertz, W. L., and R. L. Carlson (1998), An independent test of thermal subsidence and asthenosphere flow beneath the Argentine Basin, *Earth Planet. Sci. Lett.*, *161*, 73–83.

Holbrook, W. S., and P. B. Kelemen (1993), Large igneous province on the US Atlantic margin and implications for magmatism during continental break-up, *Nature*, *364*, 433–436.

Holbrook, W. S., D. Lizarralde, S. McGeary, N. Bangs, and J. Diebold (1999), Structure and composition of the Aleutian island arc and implications for continental crustal growth, *Geology*, *27*(1), 31–34.

Holbrook, W. S., et al. (2001), Mantle thermal structure and active upwelling during continental breakup in the North Atlantic, *Earth Planet. Sci. Lett.*, *190*, 251–266.

Holmes, R. C., M. Tolstoy, A. J. Harding, J. A. Orcutt, and J. Phipps Morgan (2010), Australian Antarctic Discordance as a simple mantle boundary, *Geophys. Res. Lett.*, *37*(9), L09309, doi:10.1029/2010GL042621.

Hopper, J. R., T. Dahl-Jensen, W. S. Holbrook, H. C. Larsen, D. Lizarralde, J. Korenaga, G. M. Kent, and P. B. Kelemen (2003), Structure of the SE Greenland margin from seismic relection and refraction data: Implications for nascent spreading center subsidence and asymmetric crustal accretion during North Atlantic opening, *J. Geophys. Res.*, *108*(B5), 2269, doi:10.1029/2002JB001996.

Jokat, W., O. Ritzmann, C. Reichert, and K. Hinz (2004), Deep crustal structure of the continental margin of the Explora Escarpment and in the Lazarev Sea, East Antarctica, *Mar. Geophys. Res.*, *25*(3–4), 283–304.

Jones, S. M., N. White, B. J. Clarke, E. Rowley, and K. Gallagher (2002), Present and past influence of the iceland plume on sedimentation, *Geol. Soc. London Spec. Publ.*, *196*(1), 13–25.

Kaban, M. K., P. Schwintzer, I. M. Artemieva, and W. D. Mooney (2003), Density of the continental roots: Compositional and thermal contributions, *Earth Planet. Sci. Lett.*, *209*(1–2), 53–69.

Klingelhöfer, F., L. Gáli, L. Matias, N. Steinsland, and J. Mohr (2000), Crustal structure of a super-slow spreading centre: A seismic refraction study of Mohns Ridge, 72°N, *Geophys. J. Int.*, *141*, 509–526.

Klingelhöfer, F., C. Labails, E. Cosquer, S. Rouzo, L. Géli, D. Aslanian, J. Olivet, M. Sahabi, H. Nouzé, and P. Unternehr (2008), Crustal structure of the SW-Moroccan margin from wide-angle and reflection seismic data (the DAKHLA experiment) Part A: Wide-angle seismic models, *Tectonophysics*, *468*, 63–82, doi:10.1016/j.tecto.2008.07.022.

Kopp, H., D. Klaeschen, E. R. Flueh, and J. Bialas (2002), Crustal structure of the Java margin from seismic wide-angle and multichannel reflection data, *J. Geophys. Res.*, *107*(B2), 2034, doi:10.1029/2000JB000095.

Korenaga, J., W. S. Holbrook, G. M. Kent, P. B. Kelemen, R. S. Detrick, H.-C. Larsen, J. R. Hopper, and T. Dahl-Jensen (2000), Crustal structure of the southeast Greenland margin from joint refraction and reflection seismic tomography, *J. Geophys. Res.*, *105*(B9), 21,591–21,614.

Lau, K. W. H., K. E. Louden, S. Deemer, J. Hall, J. R. Hopper, B. E. Tucholke, W. S. Holbrook, and H. C. Larsen (2006), Crustal structure across the Grand Banks-Newfoundland Basin Continental Margin—II. Results from a seismic reflection profile, *Geophys. J. Int.*, *167*, 157–170.

Levitt, D. A., and D. T. Sandwell (1995), Lithospheric bending at subduction zones based on depth soundings and satellite gravity, *J. Geophys. Res.*, *100*(B1), 379–400.

Li, C., R. D. van der Hilst, E. R. Engdahl, and S. Burdick (2008), A new global model for P wave speed variations in Earth's mantle, *Geochem. Geophys. Geosyst.*, *9*(5), Q05018, doi:10.1029/2007GC001806.

Lizzaralde, D., and W. S. Holbrook (1997), U. S. mid-Atlantic margin structure and early thermal evolution, *J. Geophys. Res.*, *102*(B10), 22,855–22,875.

Lizarralde, D., and W. S. Holbrook (2002), Crustal construction of a volcanic arc, wide-angle seismic results from the western Alaska Peninsula, *J. Geophys. Res.*, *1007*(B8), 2164, doi:10.1029/2001JB000230.

Lizarralde, D., G. J. Axen, H. E. Brown, J. M. Fletcher, A. González-Fernández, A. J. Harding, W. S. Holbrook, G. M. Kent, P. Paramo, F. Sutherland, and P. J. Umhoefer (2007), Variation in styles of rifting in the Gulf of California, *Nature*, *448*, 466–469.

Louden, K. E., and D. Chian (1999), The deep structure of non-volcanic rifted continental margins, *Philos. Trans. R. Soc. London, Ser. A*, *357*(1753), 767–800.

Lucazeau, F., et al. (2008), Persistent thermal activity at the Eastern Gulf of Aden after continental break-up, *Nat. Geosci.*, *1*, 854–858.

Marty, J., and A. Cazenave (1989), Regional variations in subsidence rate of oceanic plates: A global analysis, *Earth Planet. Sci. Lett.*, *94*(3–4), 301–315.

McBride, J. H., R. S. White, T. J. Henstock, and R. W. Hobbs (1994), Complex structure along a Mesozoic sea-floor spreading ridge: BIRPS deep seismic reflection, Cape Verde abyssal plain, *Geophys. J. Int.*, *119*, 453–478.

Miles, P. R., M. Munschy, and J. Ségoufin (1998), Structure and early evolution of the Arabian Sea and East Somali basin, *Geophys. J. Int.*, *134*, 876–888.

Minshull, T. A., and R. S. White (1996), Thin crust on the flanks of the slow-spreading Southwest Indian Ridge, *Geophys. J. Int.*, *125*(1), 139–148.

Moulin, M., D. Aslanian, J. L. Olivet, I. Contrucci, L. Matias, L. Geli, F. Klingelhoefer, H. Nouze, J. P. Rehault, and P. Unternehr (2005), Geological constraints on the evolution of the Angolan margin based on reflection and refraction seismic data (ZaïAngo project), *Geophys. J. Int.*, *162*(3), 793–810.

Müller, R. D., M. Sdrolias, C. Gaina, and W. R. Roest (2008), Age, spreading rates, and spreading asymmetry of the world's ocean crust, *Geochem. Geophys. Geosyst.*, *9*, Q04006, doi:10.1029/2007GC001743.

Navin, D. A., C. Peirce, and M. C. Sinha (1998), The RAMESSES experiment—II. Evidence for accumulated melt beneath a slow spreading ridge from wide-angle refraction and multichannel reflection seismic profiles, *Geophys. J. Int.*, *135*, 746–772.

Nyblade, A. A., and S. W. Robinson (1994), The African Superswell, *Geophys. Res. Lett.*, *21*, 765–768.

Panasyuk, S., and B. Hager (2000), Models of isostatic and dynamic topography, geoid anomalies, and their uncertainties, *J. Geophys. Res.*, *105*(B12), 28,199–28,209.

Páramo, P., W. S. Holbrook, H. E. Brown, D. Lizarralde, J. Fletcher, P. Umhoefer, G. Kent, A. Harding, A. Gonzalez, and G. Axen (2008), Seismic structure of the southern Gulf of California from Los Cabos block to the East Pacific Rise, *J. Geophys. Res.*, *113*, B03307, doi:10.1029/2007JB005113.

Parsiegla, N., J. Stankiewicz, K. Gohl, T. Ryberg, and G. Uenzelmann-Neben (2009), Southern African continental margin: Dynamic processes of a transform margin, *Geochem. Geophys. Geosyst.*, *10*(3), Q03007, doi:10.1029/2008GC002196.
Parsons, B., and J. G. Sclater (1977), An analysis of the variation of ocean floor bathymetry and heat flow with age, *J. Geophys. Res.*, *82*(5), 803–827.
Pavlenkova, N. I., V. N. Pilipenko, A. O. Verpakhovskaja, G. A. Pavlenkova, and V. P. Filonenko (2009), Crustal structure in Chile and Okhotsk Sea regions, *Tectonophysics*, *472*, 28–38.
Ranero, C., T. Reston, I. Belykh, and H. Gnibidenko (1997), Reflective oceanic crust formed at a fast-spreading center in the Pacific, *Geology*, *25* (6), 499.
Ranero, C. R., J. Phipps Morgan, K. McIntosh, and C. Reichert (2003), Bending-related faulting and mantle serpentinization at the Middle America trench, *Nature*, *425*, 367–373.
Rebesco, M., R. D. Larter, A. Camerlenghi, and P. F. Barker (1996), Giant sediment drifts on the continental rise west of the Antarctic Peninsula, *Geo-Mar. Lett.*, *16*, 65–75.
Ricard, Y., M. Richards, C. Lithgow-Bertelloni, and Y. Le Stunff (1993), A geodynamic model of mantle density heterogeneity, *J. Geophys. Res.*, *98*(B12), 21,895–21,909.
Ritsema, J., A. Deuss, H. J. van Heijst, and J. H. Woodhouse (2011), S40RTS: A degree-40 shear-velocity model for the mantle from new Rayleigh wave dispersion, teleseismic traveltime and normal-mode splitting function measurements, *Geophys. J. Int.*, *184*(3), 1223–1236, doi:10.1111/j.1365-246X.2010.04884.x.
Ritzmann, O., W. Jokat, W. Czuba, A. Guterch, R. Mjelde, and Y. Nishimura (2004), A deep seismic transect from Hovgård Ridge to northwestern Svalbard across the continental-ocean transition: A sheared margin study, *Geophys. J. Int.*, *153*, 683–702.
Roberts, G. G., J. D. Paul, N. White, and J. Winterbourne (2012), Temporal and spatial evolution of dynamic support from river profiles: A framework for Madagascar, *Geochem. Geophys. Geosyst.*, *13*(4), Q04004, doi:10.1029/2012GC004040.
Rodger, M., A. B. Watts, C. J. Greenroyd, C. Peirce, and R. W. Hobbs (2006), Evidence for unusually thin oceanic crust and strong mantle beneath the Amazon Fan, *Geology*, *34*(12), 1081–1084.
Sage, F., C. Basile, J. Mascle, B. Pontoise, and R. B. Whitmarsh (2000), Crustal structure of the continent-ocean transition of the Cote dIvoire-Ghana transform margin: Implications for thermal exchanges across the palaeotransform boundary, *Geophys. J. Int.*, *143*, 662–678.
Scherwath, M., E. Contreras-Reyes, E. R. Flueh, I. Grevemeyer, A. Krabbenhoeft, C. Papenberg, C. J. Petersen, and R. W. Weinrebe (2009), Deep lithospheric structures along the southern central Chile margin from wide-angle P-wave modelling, *Geophys. J. Int.*, *179*, 579–600.
Shillington, D. J., W. S. Holbrook, H. J. A. Van Avendonk, B. E. Tucholke, J. R. Hopper, K. E. Louden, H. C. Larsen, and G. T. Nunes (2006), Evidence for asymmetric nonvolcanic rifting and slow incipient oceanic accretion from seismic reflection data on the Newfoundland margin, *J. Geophys. Res.*, *111*(B12), B09402, doi:10.1029/2005JB003981.
Smith, W. H. F., and D. T. Sandwell (1997), Global seafloor topography from satellite altimetry and ship depth soundings, *Science*, *277*, 1957–1962.
Spasojevic, S., and M. Gurnis (2012), Sea level and vertical motion of continents from dynamic Earth models since the late Cretaceous, *AAPG Bulletin*, *96*(11), 2037–2064.
Stagg, H. M. J., M. B. Alcock, G. Bernardel, A. M. G. Moore, P. A. Symonds, and N. F. Exon (2004a), *Geological Framework of the Outer Exmouth Plateau and Adjacent Ocean Basins*, Record No. 2004/013, Geoscience Australia, Canberra.
Stagg, H. M. J., J. B. Colwell, N. G. Direen, P. E. O'Brien, B. J. Brown, G. Bernadel, I. Borissova, L. Carson, and D. B. Close (2004b), *Geological Framework of the Continental Margin in the Region of the Australian Antarctic Territory*, Record No. 2004/25, Geoscience Australia, Canberra.
Stein, C. A., and S. Stein (1992), A model for the global variation in oceanic depth and heat flow with lithospheric age, *Nature*, *359*, 123–129.
Steinberger, B. (2007), Effects of latent heat release at phase boundaries on flow in the Earth's mantle, phase boundary topography and dynamic topography at the Earth's surface, *Phys. Earth Planet. Inter.*, *164*(1–2), 2–20.
Tapley, B., et al. (2005), GGM02—An improved Earth gravity field model from GRACE, *J. Geod.*, *79*, 467–478.
Thinon, I., L. Matias, J. P. Rehault, A. Hirn, L. Fidalgo-Gonzalez, and F. Avedik (2003), Deep structure of the Armorican Basin (Bay of Biscay): A review of Norgasis seismic reflection and refraction data, *J. Geol. Soc.*, *160*(1), 99–116.
Tsikalas, F., O. Eldholm, and J. I. Faleide (2005), Crustal structure of the Lofoten-Vesterålen continental margin, of Norway, *Tectonophysics*, *404*, 151–174.
Tsuji, T., Y. Nakamura, H. Tokuyama, M. F. Coffin, and K. Koda (2007), Oceanic crust and Moho of the Pacific Plate in the eastern Ogasawara Plateau region, *Isl. Arc*, *16*(3), 361–373.
Tsuru, T., J.-O. Park, N. Takahashi, S. Kodaira, Y. Kido, Y. Kaneda, and Y. Kono (2000), Tectonic features of the Japan Trench convergent margin off Sanriku, northeastern Japan, revealed by multichannel seismic reflection data, *J. Geophys. Res.*, *105*(B7), 16,403–16,413.
Tucholke, B. E., R. E. Houtz, and W. J. Ludwig (1982), Sediment thickness and depth to basement in western North Atlantic Ocean basin, *AAPG Bulletin*, *66*, 1384–1395.
Tucholke, B. E., D. S. Sawyer, and J.-C. Sibuet (2007), Breakup of the Newfoundland-Iberia rift, in *Imaging, Mapping and Modelling Continental Lithosphere Extension and Breakup*, edited by G. D. Karner, G. Manatschal, and L. M. Pinheiro, pp. 9–46, Geol. Soc. of London, London, U. K.
Turner, I. M., C. Peirce, and M. C. Sinha (1999), Seismic imaging of the axial region of the Valu Fa Ridge, Lau Basin—The accretionary processes of an intermediate back-arc spreading ridge, *Geophys. J. Int.*, *138*, 495–519.
Wheeler, P., and N. White (2000), Quest for dynamic topography: Observations from Southeast Asia, *Geology*, *28*(11), 963–966.
White, R. S., D. McKenzie, and R. K. O'Nions (1992), Oceanic crustal thickness from seismic measurements and rare-Earth element inversions, *J. Geophys. Res.*, *97*, 19,683–19,715.
Whittaker, J. M., R. D. Müller, and M. Gurnis (2010), Development of the Australian-Antarctic depth anomaly, *Geochem. Geophys. Geosyst.*, *11*(11), Q11006, doi:10.1029/2010GC003276.
Winterbourne, J. R., A. G. Crosby, and N. J. White (2009), Depth, age and dynamic topography of oceanic lithosphere beneath heavily sedimented Atlantic margins, *Earth Planet. Sci. Lett.*, *287*, 137–151.
Wu, Y., K. E. Louden, T. Funck, H. R. Jackson, and S. A. Dehler (2006), Crustal structure of the central Nova Scotia margin off Eastern Canada, *Geophys. J. Int.*, *166*, 878–906.
Zelt, C. A., K. Sain, J. V. Naumenko, and D. S. Sawyer (2003), Assessment of crustal velocity models using seismic refraction and reflection tomography, *Geophys. J. Int.*, *153*, 609–626.